Competing influence of the Taiwan orogen and East Asian Summer Monsoon on South China Sea paleoenvironmental proxy records

Amy I. Hsieh[1,2], Shahin E. Dashtgard[1], Peter D. Clift[3,4], Li Lo[2], Romain Vaucher[5,6], and Ludvig Löwemark[2,7]

[1]Paleoclimate Records in Shallow Marine Strata (PRISMS) Research Group, Department of Earth Sciences, Simon Fraser University, Burnaby, Canada
[2]Department of Geosciences, National Taiwan University, Taipei, Taiwan
[3]Department of Earth Sciences, University College London, London, United Kingdom
[4]Department of Geology and Geophysics, Louisiana State University, Baton Rouge, USA
[5]Department of Earth Sciences, University of Geneva, Geneva, Switzerland
[6]Institute of Earth Sciences (ISTE), University of Lausanne, Geopolis, Lausanne, Switzerland
[7]Research Center for Future Earth, National Taiwan University, Taipei, Taiwan

Corresponding author: Amy I. Hsieh (amy_hsieh@sfu.ca)

Amy I. Hsieh	*0000-0002-1474-1120*
Shahin E. Dashtgard	*0000-0002-7763-2300*
Peter D. Clift	*0000-0001-6660-6388*
Li Lo	*0000-0002-2814-1476*
Romain Vaucher	*0000-0003-3051-4128*
Andrew T. Lin	*0000-0001-9284-3678*
Ludvig Löwemark	*0000-0002-3337-2367*

Abstract

Late Cenozoic changes in the intensity of the East Asian Summer Monsoon (EASM) are reconstructed using both terrestrial and marine proxy records; however, proxies from terrestrial (loess, pollen, and pedogenic isotopes) and marine environments (foraminifer assemblages, clay minerals, and magnetic properties) commonly display large discrepancies both in the direction and timing of changes in the EASM. In part, these discrepancies reflect long-term changes in paleogeography that are independent of climate variations. We assess the influence of a rapidly uplifting orogen on EASM records by comparing gamma-ray, $\delta^{13}C_{org}$, hematite/goethite, and magnetic susceptibility records from Upper Miocene–Lower Pleistocene strata of the Taiwan Western Foreland Basin to time-equivalent EASM proxy records in the South China Sea (SCS).

Prior to the emergence of modern Taiwan (~6.27–5.4 Ma), sediment in the SCS was largely derived from Eurasia. Following southwest migration of the collision zone and emergence ~5.4 Ma of proto-Taiwan the orogen became a major sediment source to the SCS. The uplift and southwest migration of Taiwan and northwest migration of Luzon resulted in the formation of southwest-flowing deep- and bottom-water currents and the SCS Branch of the Kuroshio Current. Together these currents transported sediment from Taiwan towards the SCS. The increased sediment input from Taiwan is recorded as a decline in hematite/goethite values in sediment records from the northern and central SCS. By ~3.2 Ma, continued southwest migration and growth of the Taiwan orogen resulted in the formation of the Taiwan Warm Current, which remobilized some sediment from Taiwan towards the East China Sea. Despite strengthening of deep-water currents during the Late Pliocene–Early Pleistocene, relative sediment input from Taiwan to the wider SCS decreased, with a relative increase in contributions from Eurasia and Luzon. In the southern SCS, where the Mekong River has dominated sedimentation since the Late Miocene, proxy records show no influence from the Taiwan orogen and instead reflect environmental changes in Mainland Southeast Asia driven mainly by monsoon variability. While the sedimentary records reflect tectonic- and geodynamic-driven changes in the sedimentary system from ~5.4–3.2 Ma, after ~3 Ma, proxy records show increased oscillation amplitudes, and this is consistent with the onset of Northern Hemisphere glaciation that weakened the EASM and enhanced its variability.

Our results show that a rapidly uplifting orogen has the potential to significantly impact paleoclimate records >1000 km away from the collision zone. This highlights the influence of shifting sediment sources on paleoclimate proxy records, which must be considered in interpreting past climate change from the sedimentary record.

1. Introduction

The intensity of the East Asian Summer Monsoon (EASM) has varied extensively through the late Cenozoic, although interpretations of the timing and magnitude of its intensification and weakening remains contentious and vary widely depending on the proxy data used. In part, the conflicting interpretations of EASM intensification reflects the fact that deep-marine proxy records are influenced by terrestrial environmental and marine biological production, as well as processes independent of climate (Clift 2017; Clift et al. 2014; Wang et al. 2005b). Here, we assess the influence of climate-independent controls, such as tectonic- and geodynamic-driven shifts in sediment transport mechanisms and sediment source, on EASM proxy records from the SCS. Through our data comparisons we demonstrate how seemingly contradictory datasets reflect physical and geographic controls on transport and preservation.

1.1. Overview of East Asian Summer Monsoon Records

Terrestrial vegetation records date an initial strengthening of the EASM in the Eocene, with increases since 23 Ma likely driven by progressive Himalayan and Tibetan topographic growth (Farnsworth et al. 2019; Prell and Kutzbach 1992; Sarr et al. 2022). Studies of terrestrial pollen from across China (e.g., Sun and Wang 2005), a loess–paleosol sequence at Qinan, China (Guo et al. 2002), and the occurrence of C4 plants in the SCS region (Jia et al. 2003) all suggest that warm, humid conditions started around 23 Ma. Finally, mineralogical and geochemical proxies indicate wetter and “more erosive” climates existed after 23 Ma, peaking at ~15 Ma, then weakening after 8 Ma (Clift et al. 2002; Wan et al. 2007). In contrast, the Red Clay sequences from the Chinese Loess Plateau include aeolian deposits that place the strengthening of the East Asian monsoon winds at 8–7 Ma (An et al. 2001; Ding et al. 1998; Ding et al. 2001; Sun et al. 1997; Sun et al. 1998).

Late Miocene to Pleistocene proxy records derived from sediment cores in the SCS are interpreted to record multiple phases of fluctuation in EASM intensity. Sedimentary magnetic parameters and hematite/goethite (Hm/Gt) values through Late Miocene (6.5–5.0 Ma) sedimentary strata cored at International Ocean Discovery Program (IODP) Site U1431, in the central, eastern SCS are interpreted to record a stable EASM that strengthened near 5 Ma (Gai et al. 2020). This is near-synchronous with the closure of the Central America Seaway, which resulted in a major reorganization of ocean circulation that led to the strengthening of the Atlantic meridional overturning circulation and enhanced moisture transfer to Eurasia (Haug and Tiedemann 1998; Lunt et al. 2008; Steph et al. 2010). Decreasing magnetic mineral content and increasing Hm/Gt between ~3.8–2.6 Ma through sedimentary strata at Ocean Drilling Program (ODP) Site 1148 in the northern SCS and IODP Site U1431, indicate a weakened summer monsoon, and this is attributed to global cooling and the onset of Northern Hemisphere glaciation (Gai et al. 2020).

In contrast, interpretations of EASM changes since 6.5 Ma based on clay/feldspar ratios, kaolinite/chlorite ratios, and biogenic opal mass-accumulation rate from ODP Site 1143 in the southern SCS suggest the EASM peaked in strength between 8.5–7.6 Ma and 7.1–6.2 Ma, was relatively stable from 6.2–3.5 Ma, and then intensified from 3.5–2.5 Ma (Wan et al. 2006; Wan et al. 2010a). The Hm/Gt record from ODP Site 1143 (Ao et al. 2011b; Zhang et al. 2009; Liu et al., 2019) also shows an intensification of the EASM (i.e., enhanced seasonality) during the Late Pliocene (3.5–2.5 Ma), which may be attributed to the phased uplift of the Tibetan Plateau (An et al. 2001; Sun et al. 2010). Hm/Gt records from nearby Site U1433 also indicate enhanced seasonality starting ~4 Ma (Liu et al. 2019). The local increase in EASM intensity in the southern SCS may be linked to formation of the western Pacific “warm pool” at ~4 Ma which made the southern SCS warmer than the northern/central SCS (Chaisson and Ravelo 2000; Jian et al. 2006; Li et al. 2004). Alternatively, it may reflect southward migration of the Intertropical Convergence Zone (Liu et al. 2019).

While sedimentation rates tend to be higher in tectonically active regions, resulting in more complete sedimentary archives when subsidence permits accumulation (Hsieh et al. 2023a; Vaucher et al. 2023b; Vaucher et al. 2021; Zhong et al. 2021), the observed discrepancies between EASM proxies from the SCS and surrounding land masses demonstrate that proxies can be both difficult to interpret and contradictory. Often this reflects comparison of wind-related marine upwelling proxies and terrestrial weathering and erosion proxies that are not directly comparable (Clift 2017). Proxy data used to assess EASM variability can be obscured by sedimentary processes independent of climate. In the SCS, there are multiple, major sediment sources that have evolved through time (Figure 1A). Each sediment source has distinct mineralogical and geochemical compositions that can produce “false” EASM signatures. To resolve accurate EASM proxy records, it is necessary to first identify and filter out “false” proxies that are not linked to EASM intensity (Clift et al. 2014; Wang et al. 2005b).

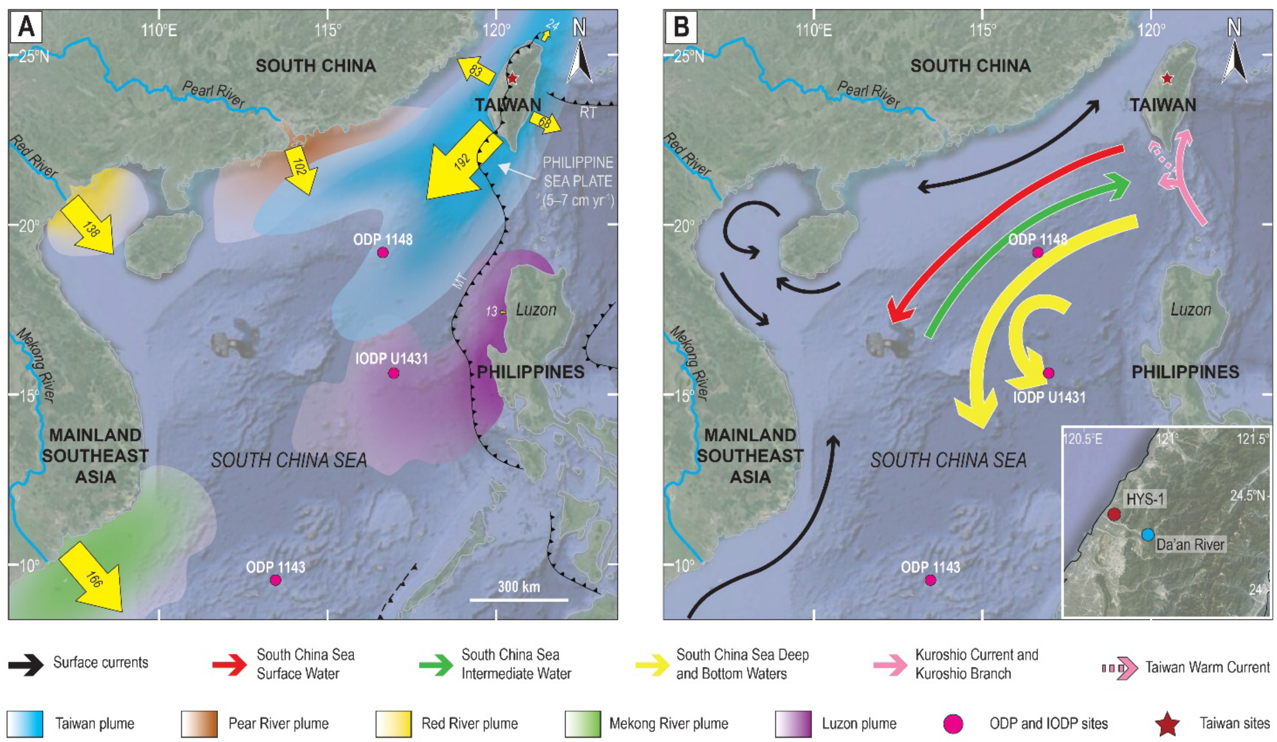

Figure 1 **A)** Simplified map showing sediment plumes (coloured polygons) into the northern and central South China Sea. Sediment plumes are modified from Liu et al. (2016) and Schroeder et al. (2015). Annual suspended pre-industrial sediment fluxes (yellow arrows) are also shown for Taiwan (Dadson et al. 2003), South China (Milliman and Farnsworth 2011; Zhang et al. 2012), Luzon (Liu et al. 2009), and Mainland Southeast Asia (Milliman and Syvitski 1992; Milliman and Farnsworth 2011), compiled by Liu et al. (2016). All values are in Mt yr^{-1} (arrow size is proportional to sediment volume). Note that the arrow from Luzon is very small. The relative translation rate of the Philippine Sea Plate with respect to the Eurasian Plate is obtained from Lin et al. (2003). **B)** Modern-day circulation in the SCS, modified from Hu et al. (2010), Liu et al. (2010a), Liu et al. (2016), and Yin et al. (2023). The locations of the Late Miocene–Early Pleistocene records used in this study are shown. The inset map in **(B)** shows the locations of the Taiwan sites, including borehole HYS-1 and the Da’an River Kueichulin Formation outcrop. MT = Manila Trench; RT = Ryuku Trench.

1.2. Oceanographic setting

The South China Sea extends over ~3.5 × 10^6 km^2. It is bound by the Asian continent to the northwest, the Indonesian and Philippine archipelagoes to the southwest and southeast, respectively, and Taiwan to the northeast (Figure 1; Wang and Li 2009). EASM proxies in the SCS region are highly sensitive to changes in 1) atmospheric circulation, 2) terrigenous input (e.g., Liu et al. 2016; Tamburini et al. 2003; Webster 1994), and 3) ocean circulation in the Pacific Ocean that passes through the Luzon Strait (e.g., Lüdmann et al. 2005; Qu 2000; Qu et al. 2006; Tian et al. 2006a). This make the SCS an area of interest for studying late Cenozoic changes in the EASM system. The SCS is situated in a tectonically active area and receives high sediment influx from various sources. Over 700 million metric tons of fluvial sediments representing approximately 3.7% of estimated global fluvial sediment discharge to the SCS (Figure 1A; Milliman and Farnsworth 2011). The main sediment sources to the SCS are the Pearl, Red, and Mekong Rivers, and rivers draining southwestern Taiwan, while small mountainous rivers in the Philippines and Indochina only contribute minor amounts (e.g., Clift et al. 2002; Liu et al. 2003; Liu et al. 2016; Milliman and Farnsworth 2011; Shao et al. 2009; Wan et al. 2007; Figure 1A). Sediment is transported subsequently across the SCS by various surface and deep-water currents (Figure 1B).

Presently, deep-water circulation in the SCS is driven by water exchange with the Pacific Ocean, which occurs through the Luzon Strait (Figure 1B; Lan et al. 2013; Tian et al. 2006b; Zhao et al. 2014). Circulation within the SCS occurs along three distinct layers (Cai et al. 2020; Lan et al. 2013; Tian et al. 2006a; Zhu et al. 2019). The SCS Surface Water (SSW) flows from the Pacific Ocean in an anticlockwise direction in the uppermost layer (0–500 m water depth) and along the Eurasian continental margin (Cai et al. 2020). The SCS Intermediate Water (SIW) flows clockwise out towards the Pacific Ocean in the middle layer (500–1500 m water depth; Cai et al. 2020; Qu et al. 1999; Tian et al. 2006a). In the lowermost layers, the SCS Deep Water (1500–2500 m water depth) and SCS Bottom Water (>2500 m) currents flow anticlockwise, and originate as overflow from the Pacific Deep Water flowing counterclockwise (Qu et al. 2006; Tian et al. 2021; Zhao et al. 2014). The SCS Deep Water and SCS Bottom Water are characterized by low velocities (0–4 cm s^{-1}) that are seasonally variable and are modulated by tides by ± 1 cm s^{-1}; they flow dominantly towards the southwest (Chen et al. 2019a; Wang et al. 2011; Zhou et al. 2017). These deep-water currents are capable of transporting sediment along the seafloor in the northern SCS, but are too weak to be erosive (Chen et al. 2019a; Zhang et al. 2014).

The Kuroshio Current is a part of the western boundary of the North Pacific Subtropical Gyre, which branches through the Luzon Strait to the north to form the Taiwan Warm Current (TWC), and to the southwest to form the South China Sea Branch of the Kuroshio (SCSBK) (Chen et al. 2020; Hu et al. 2010; Jan et al. 2002; Liang et al. 2003; Liu et al. 2021; Nan et al. 2015). Today, the TWC is responsible for remobilizing Taiwan-sourced sediment to the East China Sea (Horng and Huh 2011; Hsiung and Saito 2017; Jan et al. 2002; Kao et al. 2008; Liu et al. 2010b; Milliman et al. 2007), and the SCSBK transports sediment from Taiwan and Luzon to the northern SCS (Liu et al. 2016).

1.3. Geological setting

The Taiwan orogen formed as the result of collision between the Luzon Arc on the Philippine Sea Plate and the Eurasian Plate. The onset of arc-continent collision began as early as the Late Miocene (~12–8 Ma; Chang and Chi 1983; Clift et al. 2003; Clift et al. 2008; Tensi et al. 2006). Since that time the collision point has propagated towards the southwest (Covey 1986; Suppe 1981; Teng 1990) so that orogenesis began northeast of modern Taiwan starting ~6.5 Ma (Castelltort et al. 2011; Covey 1986; Lin and Watts 2002; Lin et al. 2003; Nagel et al. 2018; Pan et al. 2015). The Late Miocene–Pliocene (~6.3–3.2 Ma) Kueichulin Formation was deposited in the Western Foreland Basin (WFB) concurrently with uplift of the Taiwan orogen and comprises mainly shallow-marine and deltaic strata (Castelltort et al. 2011; Covey 1986; Dashtgard et al. 2021; Dashtgard et al. 2020; Lin et al. 2003; Nagel et al. 2013; Pan et al. 2015; Yu and Chou 2001). The Kueichulin Formation comprises three members (from bottom to top, Figure 2): Kuantaoshan Sandstone (~6.5–5.4 Ma), Shihliufen Shale (~5.4–4.92 Ma), and Yutengping Sandstone (~4.92–3.2 Ma) (Castelltort et al. 2011; Lin et al. 2007; Pan et al. 2015; Shaw 1996). The Kuantaoshan Sandstone is interpreted to represent deposition in water depths ranging from 25 to 35 m, (Nagel et al. 2013). The overlying Shihliufen Shale is interpreted to represent deposition in an offshore environment in water depths deeper than 35 m (Dashtgard et al. 2021; Nagel et al. 2013), and the Yutengping Sandstone is interpreted as recording deposition in water depths of 20–35 m (Dashtgard et al. 2021; Dashtgard et al. 2020; Nagel et al. 2013). Overlying the Kueichulin Formation is the <300 m thick Chinshui Shale (Late Pliocene; ~3.2–2.52 Ma), which records deposition in an offshore environment during a period of maximum flooding in the WFB (Castelltort et al. 2011; Nagel et al. 2018; Nagel et al. 2013; Pan et al. 2015; Vaucher et al. 2023b). The heterolithic Cholan Formation was deposited in the Early Pleistocene in shallow-marine environments with influence from wave, river, and tide processes (Covey 1986; Nagel et al. 2013; Pan et al. 2015; Vaucher et al. 2023a; Vaucher et al. 2021). At the top of the interval lies the Upper Pleistocene Toukoshan Formation, which comprises conglomerates deposited in terrestrial environments (Nagel et al. 2018).

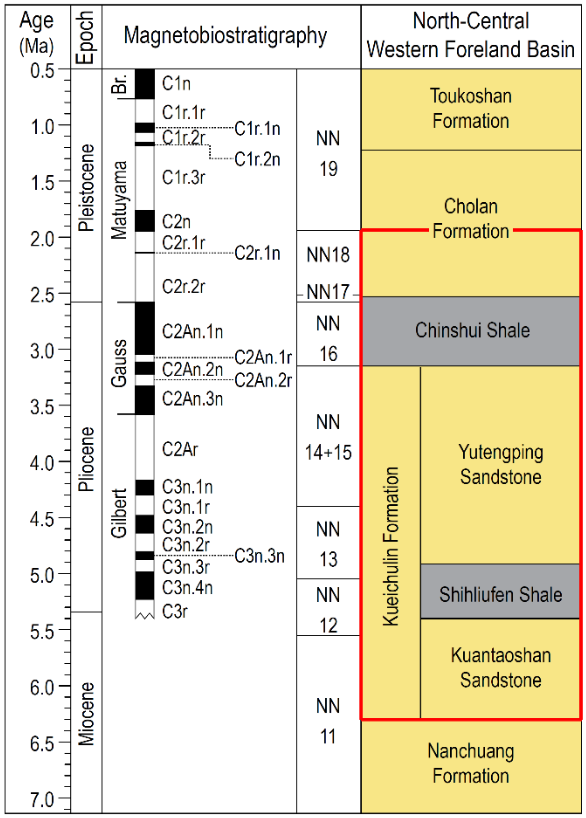

Figure 2 Chronostratigraphic correlation of sedimentary strata in the north-central extent of the WFB of Taiwan (after Teng (1990) and Chen (2016)). The Kueichulin Formation, the Chinshui Shale, and the Cholan Formation are highlighted in the red box. Yellow indicates that the main lithology is sandstone and grey indicates shale. Normal (black) and reversed (white) polarity reversals and nannofossil zonations (NN) are shown (Horng and Shea 2007; Pan et al. 2015; Vaucher et al. 2021). Br = Brunhes, which is a magnetostratigraphic polarity chron.

1.4. Provenance of South China Sea sediment

Studies of modern seafloor sediment in the SCS show that sediment composition is strongly controlled by its provenance and records the mixing of sediment from the major fluvial point sources in the region (Figure 1) (e.g., Clift et al. 2014; Clift et al. 2022; Horng and Huh 2011; Kissel et al. 2016, 2017; Liu et al. 2009; Liu et al. 2007; Liu et al. 2010b; Liu et al. 2016; Wan et al. 2010b). Modern-day fluvial sediment derived from Taiwan is characterized by low proportions of smectite and kaolinite, moderate chlorite, and high illite. In comparison, the modern Pearl, Red, and Mekong Rivers contain considerably higher proportions of kaolinite, and sediment from Luzon is dominated by smectite (Liu et al. 2016). It is noteworthy that these rivers are in a high state of anthropogenic disruption and that the Pearl River also supplied significant smectite before 2.5 ka (Hu et al. 2013). Sediment in the northern SCS reflects a Taiwanese provenance and is dominated by illite, with moderate proportions of chlorite and minor smectite and kaolinite. In contrast, sediment in the central SCS reflects a mixture of different sources, and in the east-central SCS, sediment has higher proportions of smectite due to their proximity to Luzon.

In addition to clay mineralogy, sediment from the main fluvial point sources to the SCS have distinct magnetic susceptibility (χ) signatures (Horng and Huh 2011; Kissel et al. 2016, 2017), and χ values of seafloor sediment in the SCS strongly reflect their provenance. Fluvial sediment from Taiwan contains the lowest concentrations of magnetic minerals and therefore has the lowest χ values; the dominant magnetic mineral from Taiwan is pyrrhotite (Horng and Huh 2011). Sediment from rivers discharging from South China (e.g., Pearl River) and Mainland Southeast Asia (Red and Mekong rivers) have slightly higher χ values than Taiwan. The proportion of hematite also increases southward from the Pearl River to the Mekong River (Horng and Huh 2011; Kissel et al. 2016, 2017). Sediment delivered from Luzon is enriched in magnetite and is characterized by high χ values (Horng and Huh 2011; Kissel et al. 2016, 2017). Sediment in the deep-water northern SCS (sourced mainly from Taiwanese rivers) consequently have the lowest χ values, while sediment from the east-central SCS (derived largely from Luzon) have the highest χ values.

Since its rapid uplift and exhumation Taiwan has become a major sediment source to the seas surrounding the island (Dadson et al. 2003; Dashtgard et al. 2021; Hsieh et al. 2023b; Hu et al. 2012; Hu et al. 2020; Kao et al. 2008; Kao and Milliman 2008; Liu et al. 2010b; Wan et al. 2010b). A recent study of the Upper Miocene to Lower Pliocene Kueichulin Formation in the WFB demonstrated that prior to the emergence of Taiwan in this region, sediment to the WFB (i.e., paleo-Taiwan Strait) was largely derived from Eurasia (Hsieh et al. 2023b). The onset of major sediment supply from the Taiwan orogen to the WFB began at ~5.3 Ma as the collision zone migrated into this region. This change is ~2 million years earlier than previously recognized; however, the areal distribution of these sediments is unknown. By ~4.92 Ma, Taiwan had become the dominant sediment source to the modern WFB as a result of rapid uplift and erosion and continued southwest migration of the collision zone. The shift in sediment provenance towards a Taiwan-dominated source to the WFB and SCS is independent of climate change, and hence, complicates the interpretation of EASM proxies derived from the sedimentary record.

The Hm/Gt ratio has been used as a proxy for monsoon-related precipitation in East Asia where up to 85–90% of annual rainfall occurs during the summer monsoon season (Clift 2006; Liu et al. 2007; Zhang et al. 2009). The presence of hematite is indicative of iron oxidation under arid climates, while yellow goethite forms under humid climates (e.g., Kämpf and Schwertmann 1983; Maher 1986). The seasonal character of the monsoon climate encourages hematite formation during the dry winter season (Lepre and Olsen 2021). Consequently, decreasing Hm/Gt can indicate weaker summer monsoons and increasing Hm/Gt may correspond to stronger summer monsoons. Monsoonal climates are favourable for the formation of hematite because moisture from the wet season produces ferrihydrite, while seasonal dryness is required for the formation of hematite from ferrihydrite (Balsam et al. 2004; Schwertmann 1971).

Magnetic susceptibility values can be used to determine the main source of terrigenous material delivered to the SCS as well as variations in EASM strength. Major land masses near the SCS, including Taiwan, Eurasia, and Luzon, have distinct χ values (Horng and Huh 2011; Kissel et al. 2017). Magnetic susceptibility of marine sediment is proportional to terrigenous material input, which increases with enhanced monsoon precipitation-related runoff (Clift et al. 2002; Kissel et al. 2017; Tian et al. 2005).While Hm/Gt and χ values of SCS sediment have traditionally been used as EASM rainfall proxies, they can also reflect changes in contributions from the various sediment sources to the SCS (Horng and Huh 2011; Kissel et al. 2016, 2017). $\delta^{13}C_{org}$ values of organic material have also been used as an indicator for the uplift and erosion of the Taiwan orogen (Hsieh et al. 2023b) as $\delta^{13}C_{org}$ can be used to distinguish between marine and terrestrial sources (e.g., Czarnecki et al. 2014; Dashtgard et al. 2021; Hilton et al. 2010; Kao and Liu 2000; Kao et al. 2014; Peterson and Fry 1987).

2. Study Sites and Methods

To evaluate whether variations in SCS sedimentary records are driven by changing EASM intensity or changing sediment sources, we compare variations in gamma ray (GR), $\delta^{13}C_{org}$, χ, and Hm/Gt profiles collected through Upper Miocene–Lower Pleistocene strata of the WFB in northwestern Taiwan and deep-sea sediment cores in the SCS. Gamma-ray data are from a borehole (HYS-1; 120.702024°E, 24.399908°N; Lin et al. 2007) drilled through the Kueichulin Formation, the Chinshui Shale, and the Cholan Formation of the WFB. The age-model for GR data from HYS-1 is derived from Hsieh et al. (2023b; Kueichulin Formation) and Vaucher et al. (2023b; Chinshui Shale and Cholan Formation). Values for $\delta^{13}C_{org}$ and χ were measured from samples collected from a section of the Kueichulin Formation along the Da'an River (24.29479°N, 120.91062°E; Dashtgard et al. 2021; Hsieh et al. 2023b). The HYS-1 and Da'an River sites are referred to collectively in this study as the "Taiwan sites". From the SCS, Hm/Gt and χ profiles are collected from ODP Site 1148 (18.836170°N, 116.565760°E, approximately 740 km southwest of the Taiwan sites), IODP Site U1431 (15.375818°N, 117.000015°E, approximately 1060 km southwest of the Taiwan sites), and ODP Site 1143 (9.361990°N, 113.285030°E, approximately 1830 km southwest of the Taiwan sites; Figure 1)

Variations in GR intensity recorded on wireline logs correspond largely to changes in lithology (Green and Fearon 1940; Schlumberger 1989). In siliciclastic sedimentary strata, GR values below 75 American Petroleum Institute (API) units correspond generally to sandstone-rich intervals, and GR values exceeding 105 API correspond to mudstone-rich intervals. Gamma-ray values between 75 and 105 API typically indicate heterolithic strata and/or muddy sandstone/sandy mudstone.

$\delta^{13}C_{org}$ and χ were measured from the Da'an River outcrop for time intervals 5.83–4.13 Ma ($\delta^{13}C_{org}$) and ~5.72–4.14 Ma (χ) (Hsieh et al. 2023b). Magnetic susceptibility records are available from IODP Site U1431 (Gai et al. 2020) and ODP Site 1143 (Wang et al. 2005a). Diffuse reflectance spectroscopy (DRS) was used to quantify the distribution of iron oxides such as hematite (Fe_2O_3) and oxyhydroxides such as goethite (α-FeO(OH)) in the cored successions from ODP Sites 1148 (Clift 2006) and 1143 (Ao et al. 2011a; Liu et al., 2019), and IODP Site U1431 (Gai et al. 2020). Hematite and goethite in bulk sediment strongly influences the colour intensity at the 565 and 435 nm bands, respectively, and therefore their relative abundances can be estimated using DRS (Giosan et al. 2002; Harris and Mix 1999; Harris and Mix 2002; Zhang et al. 2007).

Stratal ages in the Kueichulin Formation are based on magnetobiostratigraphic ages (Figure 2; Hsieh et al. 2023a), and magnetobiostratigraphic age boundaries are used to correlate GR, $\delta^{13}C_{org}$, and χ records from the Taiwan sites to an orbitally tuned, benthic foraminiferal, stable oxygen isotope ($\delta^{18}O$) record (Wilkens et al. 2017) from the equatorial Atlantic Ocean (Figure 3; Hsieh et al. 2023a; Vaucher et al. 2023b). The $\delta^{18}O$ record of Wilkens et al. (2017) is used for orbital tuning because it was tuned to physical sedimentary properties independent of ice volume, and has a robust timescale. Stratal ages from ODP Site 1148 are constrained using biostratigraphic ages of benthic foraminifera (Shipboard Scientific Party 2000), and stratal ages from IODP Site U1431D are magnetobiostratigraphically constrained (Gai et al. (2020). Finally, stratal ages from ODP Site 1143 are astronomically tuned by correlating the $\delta^{18}O$ record of benthic foraminifera from the same core to the LR04 stack of 57 globally distributed benthic $\delta^{18}O$ records (Ao et al. 2011b).

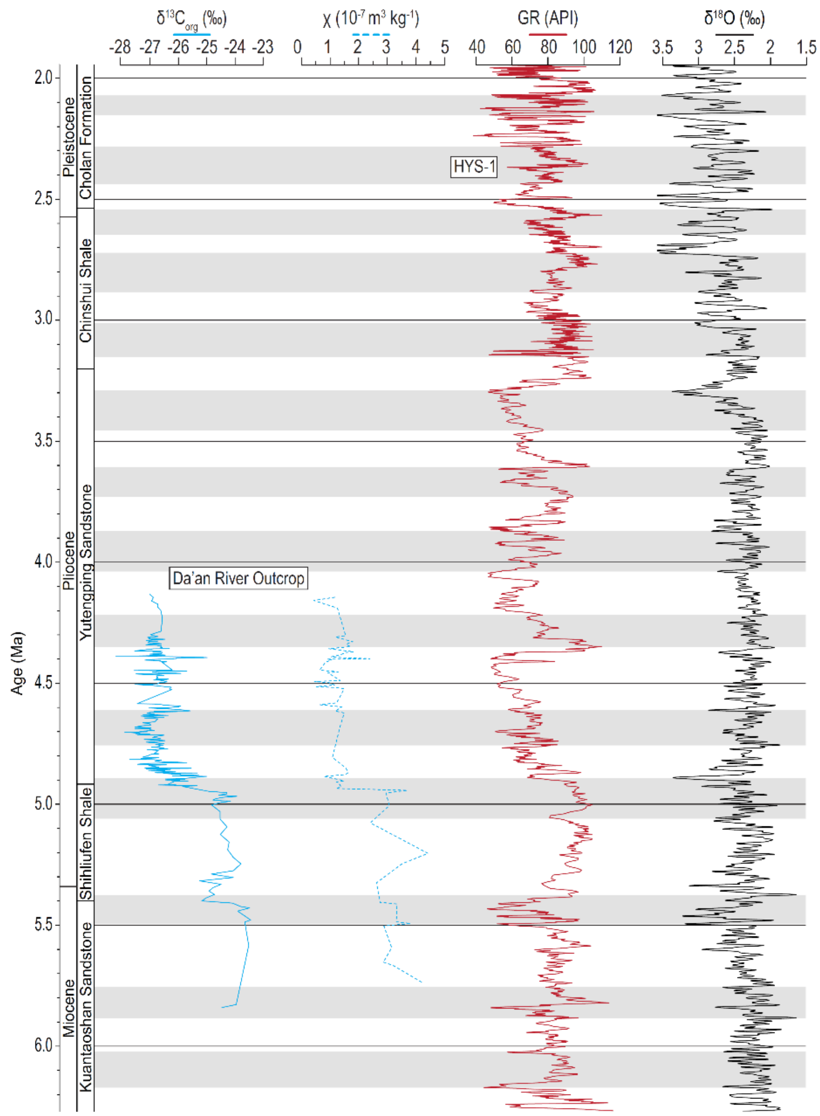

Figure 3 The benthic foraminiferal $\delta^{18}O$ record (black curve; Wilkens et al. (2017)) is used to astronologically tune and correlate the records from the Kueichulin Formation, the Chinshui Shale, and the Cholan Formation (Hsieh et al. 2023a; Vaucher et al. 2023b). Gamma-ray data (GR) from HYS-1 are from Lin et al. (2007). Organic carbon isotopic ratios ($\delta^{13}C_{org}$) are from Dashtgard et al. (2021) and Hsieh et al. (2023b), and magnetic susceptibility (χ) data from the Da'an River Kueichulin Formation outcrop are from Hsieh et al. (2023b). Selected tie points used to tune the datasets are shown by white and grey rectangles.

3. Results

3.1. Taiwan Sites

The proxies from the HYS-1 wellbore and Da'an River outcrop in northwest Taiwan show overall stable trends between ~6.27 and 5.4 Ma, with GR values of 81.1 ± 12.1 API, $\delta^{13}C_{org}$ values of -23.5 ± 0.3 ‰, and χ values of 3.4 ± 0.5 × 10^7 m^3 kg^{-1} (Figure 4). Deposition of the Shihliufen Shale occurred during the early stages of emergence of Taiwan in the modern region (~5.4–4.92 Ma), and through the Shihliufen Shale, GR values increase to a maximum of 104.9 API, while $\delta^{13}C_{org}$ and χ values decrease to lows of -

25.6 ‰ and 1.1 × 10^7 m^3 kg^{-1}, respectively. During early deposition of the Yutengping Sandstone (~4.92–4.6 Ma) GR, $\delta^{13}C_{org}$, and χ values all rapidly decrease to minimum values of 50.5 API, -27.8 ‰, and 0.7 × 10^7 m^3 kg^{-1}, respectively. Later during deposition of the Yutengping Sandstone (~4.6–3.2 Ma), all proxies stabilized overall, with GR values of 70.5 ± 13.7 API, $\delta^{13}C_{org}$ values of -26.5 ± 0.5 ‰, and χ values of 1.1 ± 0.5 × 10^7 m^3 kg^{-1}. Finally, near the top of the Yutengping Sandstone as it transitions into the Chinshui Shale (~3.2 Ma), GR values increase rapidly then stabilize at 81 ± 1.4 API. GR values remain relatively stable to the end of the record, even with increasing sand-mud variability during deposition of the Cholan Formation from ~2.52–1.95 Ma.

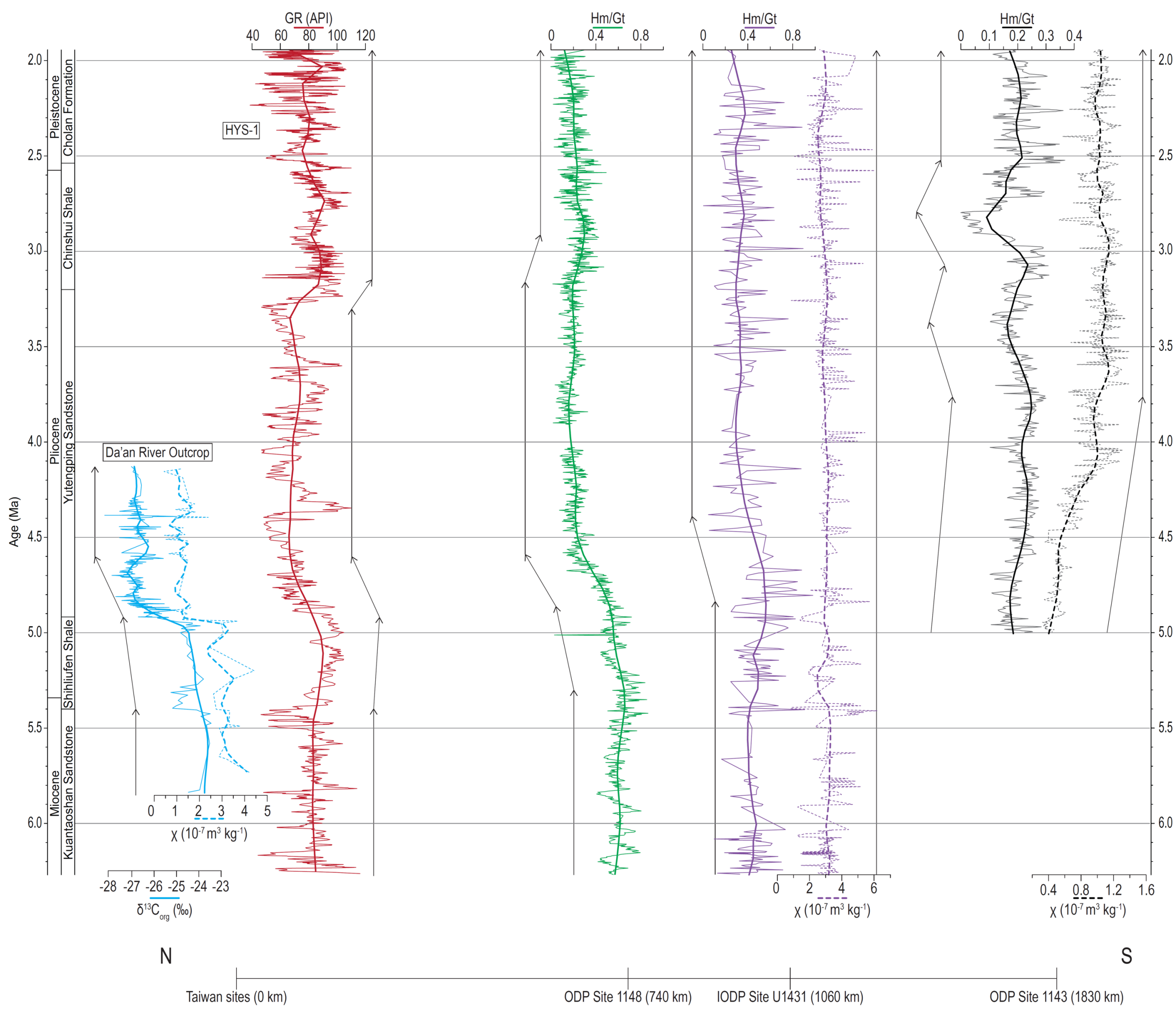

Figure 4 Compilation of $\delta^{13}C_{org}$, mass-specific magnetic susceptibillty (χ), and gamma-ray (GR) data from the Taiwan sites (Hsieh et al. 2023a; Hsieh et al. 2023b; Vaucher et al. 2023b), and East Asian Summer Monsoon proxy records from the South China Sea. Hematite/goethite (Hm/Gt) data at ODP Site 1148 are from Clift (2006); Hm/Gt and χ data at IODP Site U1431 are from Gai et al. (2020); Hm/Gt data from Ao et al. (2011b) and mass-specific magnetic susceptibiltiy (χ) from Wang et al. (2005a) for ODP Site 1143. The arrows indicate the intervals and trends discussed in the text.

3.2. ODP Site 1148

From ~6.27 to 5.3 Ma, Hm/Gt values from ODP Site 1148 were stable at 0.6 ± 0.1. From ~5.3 to 4.59 Ma, Hm/Gt began to decrease, with an anomalously low value of 0.03 at ~5.01 Ma and accelerating in its decrease near 4.87 Ma to a low of 0.1 (Figure 4). Hm/Gt stabilized between ~4.59 and ~3.18 Ma at an average of 0.2 ± 0.1. From ~3.18 to 2.91 Ma, Hm/Gt values began to increase and then stabilized after ~2.91 Ma at 0.2 ± 0.1 until the end of the record at ~1.95 Ma.

3.3. IODP Site U1431

The χ record at IODP Site U1431 shows a stable trend between ~6.27 and 1.95 Ma, averaging 7.1 ± 4 × 10^7 m^3 kg^{-1} (Figure 4). In contrast, Hm/Gt values average 0.5 ± 0.2 between ~6.27 and 4.82 Ma and began to decrease from ~4.82 to ~4.4 Ma reaching a minimum of 0.04. Between ~4.4 and 1.95 Ma, Hm/Gt values remained relatively stable, averaging 0.4 ± 0.2.

3.4. ODP Site 1143

At ODP Site 1143, both the Hm/Gt and χ records show increasing trends from the start of the record at ~5 to ~3.77 Ma, reaching maximum values of 0.3 and 1.4 × 10^7 m^3 kg^{-1}, respectively (Figure 4). From ~3.77 to 2.52 Ma, Hm/Gt showed two fluctuating cycles, with a minimum of 0.1 at ~3.37 Ma and a maximum of 0.3 at ~3.13 Ma, followed by another minimum of 0 at ~2.8 Ma and maximum of 0.4 at ~2.53 Ma. After ~2.52 Ma Hm/Gt stabilized to an average of 0.2 ± 0.1. In contrast, χ remains relatively stable from ~3.77 to 1.95 Ma, averaging 1.0 ± 0.1 × 10^7 m^3 kg^{-1}.

4. Discussion

4.1. Late Miocene (~6.27–5.4 Ma): early stages of arc-continent collision

During the early stages of collision between the Eurasian Plate and Luzon Arc in the modern Taiwan area and prior to its emergence (~6.27–5.4 Ma), sediment delivered to the northern and central SCS was derived largely from rivers discharging from the Eurasian continental margin (i.e., present-day South China and Mainland Southeast Asia). The redistribution of terrestrially derived sediment in the marine realm is reflected in the $\delta^{13}C_{org}$ record through the Kuantaoshan Sandstone where values lower than -24 ‰ suggest a long residence time of sediment on the seafloor and incorporation of significant volumes of marine organic matter (Dashtgard et al. 2021; Hsieh et al. 2023b). Gamma-ray values measured through the Kuantaoshan Sandstone also reflect deposition of sand-dominated sediment, probably in water depths of 25–35 m (Figure 5; Nagel et al. 2013). Magnetic susceptibility values are also high and stable through this time period both at the Taiwan sites and at IODP Site U1431, and this reflects sediment derivation largely from Eurasia (i.e., South China and Mainland Southeast Asia; Figure 5; Horng and Huh 2011; Kissel et al. 2016, 2017). The Hm/Gt records at both ODP Site 1148 and IODP Site U1431 are also stable during this time period, which is consistent with a dominant Eurasian source enriched in hematite under stable environmental conditions (Horng and Huh 2011; Kissel et al. 2016, 2017).

Sediment contributions to the northern and central SCS from other sources besides Eurasia between ~6.27 and 5.4 Ma were probably insignificant. Contributions from the Philippines during this period were probably lower than the present day because the archipelago was located in a more distal position compared to now (Figure 6; Hall 1996, 2002; Lee and Lawver 1994). As well, during the Late Miocene, prior to emergence of Taiwan (Chen et al. 2019b; Covey 1986; Lin and Watts 2002; Lin et al. 2003) and when Luzon was southeast of its present position (Clift et al. 2008; Hall 1996, 2002, 2012; Lee and Lawver 1994), the SCS was open to the Pacific Ocean (Figure 6; Wang and Li 2009; Yin et al. 2021). Paleocurrents inferred from contourites indicate that in the Late Miocene, the SCS shared the same circulation pattern as the North Pacific Subtropical Gyre with a dominant clockwise flow direction (Yin et al. 2021; Yin et al. 2023; Figure 6A). Sediment deposited in the SCS during this time would reflect provenance from the Eurasian margin and dispersal by paleo-SCS currents.

4.2. Late Miocene to middle Pliocene (5.4–3.2 Ma): emergence of Taiwan

As the collision zone between the Eurasian Plate and the Luzon Arc migrated southwestwards and modern Taiwan began to emerge (i.e., subaerially exposed) near 5.4 Ma, the island rapidly became a significant sediment source to the WFB (Figure 5; Hsieh et al. 2023b). The impact of Taiwan on sedimentation in the WFB is recorded by the gradual decrease in $\delta^{13}C_{org}$ and χ values from ~5.4 to 4.92 Ma, which reflect increases in both terrestrial organic content (from plants and soil) and low-χ sediment derived from erosion of metasedimentary rocks of the Taiwan orogen (Hsieh et al. 2023b). GR values were high between ~5.4 and 4.92 Ma reflecting deposition of the Shihliufen Shale at increasing water depths as the WFB subsided. Sediment export from Taiwan to the WFB begins to accelerate at ~4.92 Ma and reached a maximum between ~4.6 Ma and 3.2 Ma as Taiwan became the dominant source of sediment to the basin (Hsieh et al. 2023b). This is manifested in the abrupt decrease in the $\delta^{13}C_{org}$ and χ values near the top of the Shihliufen Shale and into the base of the Yutengping Sandstone in the Taiwan sites (Figure 5). GR values also abruptly decreased after ~4.92 Ma, reflecting rapid deposition of sand-dominated sediment exported from Taiwan.

The export of large volumes of low-χ, sand-dominated sediment with high terrestrial organic content is attributed largely to tropical cyclones denuding Taiwan (Dashtgard et al. 2021; Hsieh et al. 2023b; Vaucher et al. 2023a; Vaucher et al. 2021). Tropical cyclones were probably more frequent and more intense during the Pliocene because of the warmer climate (Coumou and Rahmstorf 2012; Fedorov et al. 2013; Kossin et al. 2020; Yan et al. 2019a; Yan et al. 2019b; Yan et al. 2016). Furthermore, precipitation would have been significantly enhanced if tropical cyclones coincided with EASM circulation (Chen et al. 2010; Chien and Kuo 2011; Kao and Milliman 2008; Lee et al. 2015; Liu et al. 2008). Warmer periods in the northwest Pacific since emergence of Taiwan should be manifest as higher sediment loads to the WFB.

The southwest migration of Taiwan caused by the northwest migration of Luzon combined to form the Luzon Strait, a gateway through which deep-water bottom currents enter the SCS from the Pacific Ocean (Figure 6; e.g., Caruso et al. 2006; Liu et al. 2016; Qu et al. 2006; Qu et al. 2004; Wan et al. 2010b; Wang et al. 2011; Webster 1994; Zhao et al. 2014). Bottom currents entering the SCS are then deflected to the southwest along the Eurasian continental margin and towards the central SCS (Qu et al. 2006; Qu et al. 2004; Wang et al. 2011; Zhao et al. 2014). Bottom currents bring sediment eroded from Taiwan and transported down the continental slope towards the northern/central SCS (Liu et al. 2016). The emergence of Taiwan also created the westward-flowing SCSBK, which is responsible for delivering sediment from Taiwan and the Philippines (i.e., Luzon) to the northern SCS (Liu et al. 2016). However, sediment contributions from the Philippines to the SCS today are low and this was probably similar or less during the Pliocene (Liu et al. 2009). Sediment from the other major sediment source in the northern SCS, the Pearl River, is now transported westward along the continental margin by surface currents (Liu et al. 2016; Schroeder et al. 2015), and this limits its contribution to the deep-water extent of the SCS relative to Taiwan.

Taiwan-sourced sediment exported to the SCS by deep-water bottom currents and the SCSBK (Figure 6) is depleted in hematite and enriched in pyrrhotite (Horng and Huh 2011). As Taiwan became the major sediment source to the WFB around 4.92 Ma, the rapid uplift and erosion of Taiwan resulted in increased sediment delivery to the SCS. In the northern SCS, the effect of increasing sediment supply from Taiwan is manifested at ODP Site 1148, where the Hm/Gt signal shows an accelerated decrease at ~4.87 Ma (Figure 5). By ~4.82 Ma, the effects of sediment flux from Taiwan were reflected in the central SCS, wherein the Hm/Gt record from IODP Site U1431 also began to decrease (Figure 5). The delayed response times between ODP Site 1148 and IODP Site U1431 is probably due to their position relative to Taiwan, but we cannot rule out uncertainties in the age models. Average Hm/Gt values at IODP Site U1431 are higher than at ODP Site 1148 which is interpreted to reflect their relative distances from Taiwan (hematite-depleted sediment source) and Eurasia (hematite-enriched sediment source). This interpretation is supported by the relatively stable χ values at IODP Site U1431 before and after 4.82 Ma, which probably records mixing of sediment sourced from Taiwan, Eurasia, and Luzon, each of which have distinct χ values (Horng and Huh 2011; Kissel et al. 2016, 2017). By ~4.6 Ma, sediment at both sites in the northern and central SCS reflected a dominant flux from Taiwan (Figure 5). This is attributed to both the accelerated uplift/erosion of Taiwan and to strengthening of deep-water bottom currents and the SCSBK (Figure 6).

In contrast to the northern and central SCS sites, the records from ODP Site 1143 show trends that suggest the southern SCS received limited sediment volumes from the Taiwan orogen (Figure 5). Magnetic susceptibility values are lower at ODP Site 1143 compared to IODP U1431 in the central SCS, indicating limited sediment contribution from Luzon. Instead, mineralogical and geochemical records from ODP Site 1143 indicate that since the Pliocene the Mekong River has dominated sedimentation in the southern SCS (Liu et al. 2017; Milliman and Meade 1983; Milliman and Syvitski 1992; Wan et al. 2006). Because the sediment source to the southern SCS has remained stable since the Pliocene, it is possible that the main driver of variations in Hm/Gt and χ values seen in ODP Site 1143 are related to environmental changes in Mainland Southeast Asia driven by monsoon variability (Ao et al. 2011b; Wan et al. 2006; Wan et al. 2010a; Zhang et al. 2009).

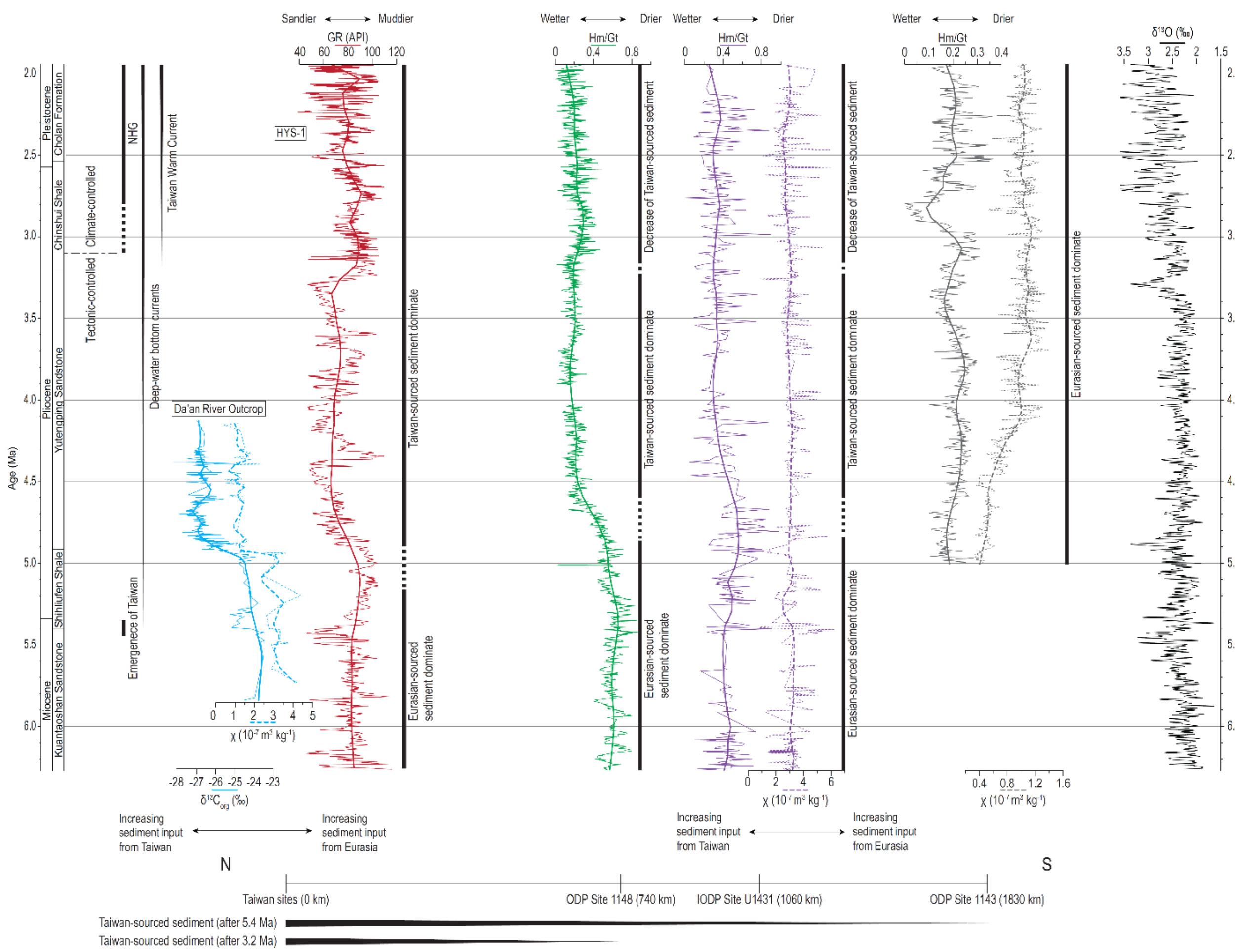

Figure 5 Chronostratigraphic cross-section from north (N) to south (S) with the interpreted extent of sediment distribution from the Taiwan orogen and key tectonic and climatic events and changes in ocean circulation.

4.3. Late Pliocene–Early Pleistocene (after ~3.2 Ma): Subsidence of the WFB and current intensified flow through the Taiwan Strait

As the Taiwan orogen continued to grow and propagate towards the southwest, the WFB experienced increasingly rapid subsidence (Lin and Watts 2002; Nagel et al. 2018; Nagel et al. 2013; Pan et al. 2015). At the same time, Luzon continued to migrate to the northwest at an increasingly faster rate. Together the movement of these two land masses narrowed and shallowed the Luzon Strait (Hall 1996, 2002; Lee and Lawver 1994; Sibuet and Hsu 2004; Yin et al. 2023). The reduced width and depth of the Luzon Strait weakened surface and intermediate water flow, while deep-water and bottom-water currents strengthened in the SCS (Figure 6; Yin et al. 2023).

The growth of the Taiwan orogen and the formation of the Taiwan Strait resulted in the formation of alongshore currents, including the TWC flowing north along the west coast of Taiwan (Chen et al. 2020; Hu et al. 2010; Jan et al. 2002; Liang et al. 2003; Liu et al. 2021; Nan et al. 2015; Figure 6). The TWC would have remobilized sediment from Taiwan northwards to the East China Sea as it does in the present day (Horng and Huh 2011; Hsiung and Saito 2017; Jan et al. 2002; Kao et al. 2008; Liu et al. 2010b; Milliman et al. 2007). As the Taiwan orogen continued to grow, the TWC would have intensified, leading to greater northward transport of sediment. Additionally, an increase in the intensity and frequency of tropical cyclones has been shown to drive strengthening of the Kuroshio Current (Zhang et al. 2020). In the Late Pliocene, the warmer climate would have been favourable for increased tropical cyclone formation (Coumou and Rahmstorf 2012; Fedorov et al. 2013; Kossin et al. 2020; Yan et al. 2019a; Yan et al. 2019b; Yan et al. 2016), leading to a strengthening of the Kuroshio Current which enhanced northward transport of sediment from Taiwan. A decrease in sediment input from Taiwan to the SCS would result in an increase in the relative sediment contribution from Eurasia and Luzon throughout the SCS, which would be reflected in an increase in Hm/Gt at ODP Site 1148 at ~3.18–2.91 Ma.

Since the Late Pliocene, the morphological and tectonic configuration, as well as local ocean circulation of the study area likely remained relatively constant (Hall 1996, 2002; Lin et al. 2003; Yin et al. 2023), however, there was a marked intensification of Northern Hemisphere Glaciation (NHG) between ~3.1 and 2.8 Ma, (Berends et al. 2021; Haug and Tiedemann 1998; Miller et al. 2020; Raymo 1994; Shackleton et al. 1984). Expansion of the Arctic ice-sheet caused the winter monsoon to intensify and the summer monsoon to weaken in East Asia, which resulted in decreased precipitation and enhanced aridification over the past ~3 Ma (An et al. 2001; Ge et al. 2013; Prell and Kutzbach 1992; Wan et al. 2007; Wang et al. 2019; Xin et al. 2020; Zhou et al. 2023). The cooler, drier global climate is favourable for the formation of hematite (Kämpf and Schwertmann 1983; Lepre and Olsen 2021) and may also have contributed to the increase in Hm/Gt at ODP Site 1148. The Hm/Gt record at ODP Site 1143 also shows a long-term increasing trend from 2.8 to 1.95 Ma, suggesting decreasing EASM intensity. Because the Asian monsoon system is sensitive to Northern Hemisphere ice volume, sustained glaciation would also have increased the variability in monsoon strength (Ao et al. 2011b; Demenocal and Rind 1993; Prell and Kutzbach 1992). This is reflected in all the records, which show higher oscillation amplitudes after ~3 Ma, except at IODP Site U1431, where a low sample density may not have been sufficient to capture the variations. Therefore, prior to ~3 Ma, the studied records reflect largely tectonic- and geodynamic-driven shifts in sediment transport mechanisms and sediment source. After ~3 Ma, the fluctuations and amplitudes recorded in all records likely reflects climate-driven changes related to the NHG.

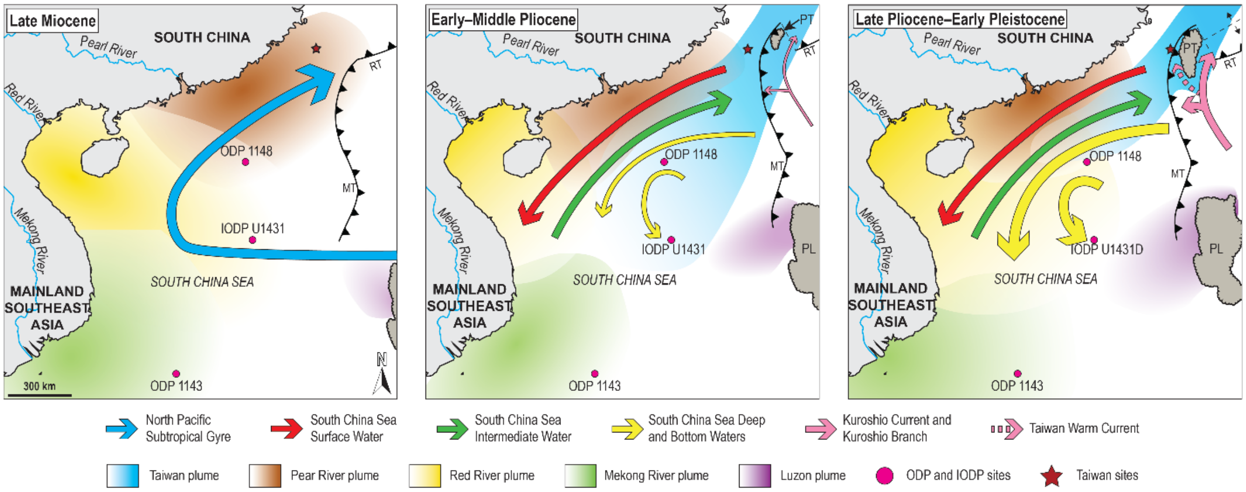

Figure 6 Late-Miocene–Early Pleistocene reconstructions of the SCS region. Geographic locations of land masses are modified from Hall (2012). Miocene ocean currents are modified from Karl (1999). Plio–Pleistocene ocean currents are based on modern-day circulation in the SCS, and are modified from Hu et al. (2010), Liu et al. (2010a), Liu et al. (2016), Schroeder et al. (2015), Yin et al. (2021), and Yin et al. (2023). The opacity of the plume colours are relative to estimated sediment contribution. PL = Proto-Luzon; PT = Proto-Taiwan.

5. Conclusion

Variations in deep-sea EASM proxies are commonly attributed to changes in climate because proxies are assumed to record changes in terrestrial weathering conditions only. Variations in proxy signals driven by shifts in sediment sources or transport processes (independent of climate) are often overlooked. Our study of sediment source characteristics combined with observed and predicted oceanic circulation in the SCS showcases that shifting sediment provenance can significantly impact proxy signals in the deep sea, and that EASM proxies should not be interpreted without consideration of sediment provenance.

Prior to emergence of the Taiwan orogen in its modern location (~6.27–5.4 Ma), Eurasia (i.e., South China and Mainland Southeast Asia) was the main sediment source to the SCS, and these sediments were dispersed by Pacific Ocean currents. Soon after the onset of major sediment supply to the SCS from Taiwan after ~5.4 Ma, sedimentary archives from the northern and central SCS shows decreasing trends in Hm/Gt values, and this reflects the introduction of large volumes of hematite-depleted sediment from Taiwan. The emergence and southwest propagation of the Taiwan orogen and the northwest migration of Luzon created both the Luzon Strait and deep-water bottom currents and the SCSBK that transported large volumes of sediment from Taiwan southwestwards to the northern and central SCS. As the Luzon Strait narrowed and shallowed with continued migration of the Taiwan orogen and Luzon, the deep-water bottom currents and therefore sediment volume delivered to the SCS from Taiwan also accelerated. The continued growth and southwest migration of the Taiwan orogen in the Late Pliocene (~3.2 Ma) resulted in the formation of the TWC, which remobilized sediment from Taiwan northwards to the East China Sea. Despite strengthening deep-water and bottom currents during this time, sediment input from Taiwan to the wider SCS decreased, and relative sediment contribution from Eurasia and Luzon dominated. In the southern SCS, where the Mekong River has dominated sedimentation since the Late Miocene, the sedimentary record appears to be largely unaffected by the evolution of Taiwan, and rather is driven by changes in EASM intensity (Liu et al. 2017). Additionally, since the Late Pliocene, the morphology, tectonic configuration, and ocean circulation of the study area remained largely unchanged, while the Northern Hemisphere glaciation intensified. This is also reflected in the studied records, in which the oscillation amplitudes reflect tectonic- and geodynamic-driven shifts prior to ~3 Ma, and climate-driven changes related to Northern Hemisphere glaciation after 3 Ma, which is consistent with enhanced variability in monsoon strength driven by sustained glaciation.

Through this comparison, we show that a rapidly uplifting orogen can significantly influence various deep-sea climate proxy records located > 1000 km away from the orogen. The influence of shifting sediment sources through time on different climate proxies emphasizes the need to consider and identify non-climate-controlled mechanisms that can drive changes in proxy records. This enables the accurate identification and interpretation of climate signals preserved in sedimentary archives, especially in tectonically active and geologically diverse regions.

Acknowledgements

We would like to thank Dr. Andrew T. Lin for providing the gamma-ray data from borehole HYS-1 used in this study. This research was supported financially through a Natural Sciences and Engineering Research Council (NSERC) of Canada Postgraduate Doctoral Scholarship (569850-2022) awarded to A.I. Hsieh and a NSERC Discovery Grant to S.E. Dashtgard (RGPIN-2019-04528). L. Löwemark acknowledges support from the Ministry of Science and Technology (MOST 111-2116-M-002-038-) and “The Featured Areas Research Center Program” within the framework of the Higher Education Sprout Project by the Ministry of Education in Taiwan. (NTU-111L901001). P. Clift thanks the Charles T. McCord Chair in Petroleum Geology for support. We are grateful for reviewers ________ and the editor _____, whose constructive feedback helped to improve this manuscript.

Conflict of interest

The authors declare no conflict of interest.

Author contributions

A.I.H. and S.E.D. were responsible for the design and conceptualization of this study. A.I.H. was responsible for data analysis and drafting of the manuscript. P.D.C., L. Lo, and L. Löwemark provided expert support in the interpretation of paleo-oceanic and paleoclimatic environments. R.V. provided expertise on the interpretation of depositional environments. All co-authors reviewed and approved the manuscript.

References

An, Z., Kutzbach, J.E., Prell, W.L., and Porter, S.C. 2001. Evolution of Asian monsoons and phased uplift of the Himalaya-Tibetan Plateau since late Miocene times. Nature, **411**: 62-66. doi:10.1038/35075035.

Ao, H., Dekkers, M.J., Qin, L., and Xiao, G. 2011a. (Table S2) Hematite/Goethite ratio and benthic $\delta^{18}O$ data of the ODP Site 184-1143 expressed on the A2011 timescale. PANGAEA.

Ao, H., Dekkers, M.J., Qin, L., and Xiao, G. 2011b. An updated astronomical timescale for the Plio-Pleistocene deposits from South China Sea and new insights into Asian monsoon evolution. Quaternary Science Reviews, **30**: 1560-1575. doi:10.1016/j.quascirev.2011.04.009.

Balsam, W., Ji, J., and Chen, J. 2004. Climatic interpretation of the Luochuan and Lingtai loess sections, China, based on changing iron oxide mineralogy and magnetic susceptibility. Earth and Planetary Science Letters, **223**: 335-348. doi:10.1016/j.epsl.2004.04.023.

Berends, C.J., de Boer, B., and van de Wal, R.S.W. 2021. Reconstructing the evolution of ice sheets, sea level, and atmospheric CO_2 during the past 3.6 million years. Climate of the Past, **17**: 361-377. doi:10.5194/cp-17-361-2021.

Cai, Z., Gan, J., Liu, Z., Hui, C.R., and Li, J. 2020. Progress on the formation dynamics of the layered circulation in the South China Sea. Progress in Oceanography, **181**: 102246. doi:10.1016/j.pocean.2019.102246.

Caruso, M.J., Gawarkiewicz, G.G., and Beardsley, R.C. 2006. Interannual variability of the Kuroshio intrusion in the South China Sea. Journal of Oceanography, **62**: 559-575. doi:10.1007/s10872-006-0076-0.

Castelltort, S., Nagel, S., Mouthereau, F., Lin, A.T.-S., Wetzel, A., Kaus, B., Willett, S., Chiang, S.-P., and Chiu, W.-Y. 2011. Sedimentology of early Pliocene sandstones in the south-western Taiwan foreland: Implications for basin physiography in the early stages of collision. Journal of Asian Earth Sciences, **40**: 52-71. doi:10.1016/j.jseaes.2010.09.005.

Chaisson, W.P., and Ravelo, A.C. 2000. Pliocene development of the east-west hydrographic gradient in the equatorial Pacific. Paleoceanography, **15**: 497-505. doi:10.1029/1999PA000442.

Chang, S.S.L., and Chi, W.-R. 1983. Neogene nannoplankton biostratigraphy in Taiwan and the tectonic implications. Petroleum Geology of Taiwan, **19**: 93-147.

Chen, D., Lian, E., Shu, Y., Yang, S., Li, Y., Li, C., Liu, P., and Su, N. 2020. Origin of the springtime South China Sea Warm Current in the southwestern Taiwan Strait: Evidence from seawater oxygen isotope. Sci. China Earth Sci, **63**: 1564-1576. doi:10.1007/s11430-019-9642-8.

Chen, H., Zhang, W., Xie, X., and Ren, J. 2019a. Sediment dynamics driven by contour currents and mesoscale eddies along continental slope: A case study of the northern South China Sea. Marine Geology, **409**: 48-66. doi:10.1016/j.margeo.2018.12.012.

Chen, J.-M., Li, T., and Shih, C.-F. 2010. Tropical Cyclone- and Monsoon-Induced Rainfall Variability in Taiwan. Journal of Climate, **23**: 4107-4120. doi:10.1175/2010jcli3355.1.

Chen, W.-S. 2016. An Introduction to the Geology of Taiwan. Geologic Society of Taiwan, Taipei, Taiwan.

Chen, W.-S., Yeh, J.-J., and Syu, S.-J. 2019b. Late Cenozoic exhumation and erosion of the Taiwan orogenic belt: New insights from petrographic analysis of foreland basin sediments and thermochronological dating on the metamorphic orogenic wedge. Tectonophysics, **750**: 56-69. doi:10.1016/j.tecto.2018.09.003.

Chien, F.-C., and Kuo, H.-C. 2011. On the extreme rainfall of Typhoon Morakot (2009). Journal of Geophysical Research, **116**. doi:10.1029/2010jd015092.

Clift, P.D. 2006. Controls on the erosion of Cenozoic Asia and the flux of clastic sediment to the ocean. Earth and Planetary Science Letters, **241**: 571-580. doi:10.1016/j.epsl.2005.11.028.

Clift, P.D. 2017. Cenozoic sedimentary records of climate-tectonic coupling in the Western Himalaya. Prog Earth Planet Sci, **4**: 1-22. doi:10.1186/s40645-017-0151-8.

Clift, P.D., Schouten, H., and Draut, A.E. 2003. A general model of arc-continent collision and subduction polarity reversal from Taiwan and the Irish Caledonides. Geological Society special publication, **219**: 81-98. doi:10.1144/GSL.SP.2003.219.01.04.

Clift, P.D., Wan, S., and Blusztajn, J. 2014. Reconstructing chemical weathering, physical erosion and monsoon intensity since 25Ma in the northern South China Sea: A review of competing proxies. Earth-Science Reviews, **130**: 86-102. doi:10.1016/j.earscirev.2014.01.002.

Clift, P.D., Lee, J.I., Clark, M.K., and Blusztajn, J. 2002. Erosional response of South China to arc rifting and monsoonal strengthening; a record from the South China Sea. Marine Geology, **184**: 207-226. doi:10.1016/S0025-3227(01)00301-2.

Clift, P.D., Lin, A.T., Carter, A., Wu, F., Draut, A., Lai, T.-H., Fei, L.-Y., Schouten, H., and Teng, L. 2008. Post-collisional collapse in the wake of migrating arc-continent collision in the Ilan Basin, Taiwan. Special Paper of the Geological Society of America, **436**: 257-278. doi:10.1130/2008.2436(12).

Clift, P.D., Betzler, C., Clemens, S.C., Christensen, B., Eberli, G.P., France-Lanord, C., Gallagher, S., Holbourn, A., Kuhnt, W., Murray, R.W., Rosenthal, Y., Tada, R., and Wan, S. 2022. A synthesis of monsoon exploration in the Asian marginal seas. Scientific Drilling, **31**: 1-29. doi:10.5194/sd-31-1-2022.

Coumou, D., and Rahmstorf, S. 2012. A decade of weather extremes. Nature Climate Change, **2**: 491-496. doi:10.1038/nclimate1452.

Covey, M. 1986. The evolution of foreland basins to steady state: Evidence from the western Taiwan foreland basin. *In* Foreland Basins. *Edited by* P.A. Allen and P. Homewood. Blackwell Publishing Ltd. pp. 77-90.

Czarnecki, J.M., Dashtgard, S.E., Pospelova, V., Mathewes, R.W., and MacEachern, J.A. 2014. Palynology and geochemistry of channel-margin sediments across the tidal–fluvial transition, lower Fraser River, Canada: Implications for the rock record. Marine and Petroleum Geology, **51**: 152-166. doi:10.1016/j.marpetgeo.2013.12.008.

Dadson, S.J., Hovius, N., Chen, H., Dade, W.B., Hsieh, M.-L., Willett, S.D., Hu, J.-C., Horng, M.-J., Chen, M.-C., Stark, C.P., Lague, D., and Lin, J.-C. 2003. Links between erosion, runoff variability and seismicity in the Taiwan orogen. Nature, **426**: 648-651. doi:10.1038/nature02150.

Dashtgard, S.E., Löwemark, L., Wang, P.-L., Setiaji, R.A., and Vaucher, R. 2021. Geochemical evidence of tropical cyclone controls on shallow-marine sedimentation (Pliocene, Taiwan). Geology, **49**: 566-570. doi:10.1130/g48586.1.

Dashtgard, S.E., Löwemark, L., Vaucher, R., Pan, Y.-Y., Pilarczyk, J.E., and Castelltort, S. 2020. Tropical cyclone deposits in the Pliocene Taiwan Strait: Processes, examples, and conceptual model. Sedimentary Geology, **405**. doi:10.1016/j.sedgeo.2020.105687.

Demenocal, P.B., and Rind, D. 1993. Sensitivity of Asian and African climate to variations in seasonal insolation, glacial ice cover, sea surface temperature, and Asian orography. J. Geophys. Res, **98**: 7265-7287. doi:10.1029/92JD02924.

Ding, Z.L., Sun, J.M., Yang, S.L., and Liu, T.S. 1998. Preliminary magnetostratigraphy of a thick eolian red clay-loess sequence at Lingtai, the Chinese Loess Plateau. Geophysical Research Letters, **25**: 1225-1228. doi:10.1029/98GL00836.

Ding, Z.L., Yang, S.L., Sun, J.M., and Liu, T.S. 2001. Iron geochemistry of loess and red clay deposits in the Chinese Loess Plateau and implications for long-term Asian monsoon evolution in the last 7.0 Ma. Earth and Planetary Science Letters, **185**: 99-109. doi:10.1016/S0012-821X(00)00366-6.

Farnsworth, A., Lunt, D.J., Robinson, S.A., Valdes, P.J., Roberts, W.H.G., Clift, P.D., Markwick, P., Su, T., Wrobel, N., Bragg, F., Kelland, S.-J., and Pancost, R.D. 2019. Past East Asian monsoon evolution controlled by paleogeography, not CO-$_2$. Science Advances, **5**: eaax1697. doi:10.1126/sciadv.aax1697.

Fedorov, A.V., Brierley, C.M., Lawrence, K.T., Liu, Z., Dekens, P.S., and Ravelo, A.C. 2013. Patterns and mechanisms of early Pliocene warmth. Nature, **496**: 43-49. doi:10.1038/nature12003.

Gai, C., Liu, Q., Roberts, A.P., Chou, Y., Zhao, X., Jiang, Z., and Liu, J. 2020. East Asian monsoon evolution since the late Miocene from the South China Sea. Earth and Planetary Science Letters, **530**. doi:10.1016/j.epsl.2019.115960.

Ge, J., Dai, Y., Zhang, Z., Zhao, D., Li, Q., Zhang, Y., Yi, L., Wu, H., Oldfield, F., and Guo, Z. 2013. Major changes in East Asian climate in the mid-Pliocene: Triggered by the uplift of the Tibetan Plateau or global cooling? Journal of Asian Earth Sciences, **69**: 48-59. doi:10.1016/j.jseaes.2012.10.009.

Giosan, L., Flood, R.D., Grützner, J., and Mudie, P. 2002. Paleoceanographic significance of sediment color on western North Atlantic Drifts: II. Late Pliocene–Pleistocene sedimentation. Marine Geology, **189**: 43-61. doi:10.1016/S0025-3227(02)00322-5.

Green, W.G., and Fearon, R.E. 1940. Well logging by radioactivity. Geophysics, **5**: 272-283.

Guo, Z.T., Ruddiman, W.F., Hao, Q.Z., Wu, H.B., Qiao, Y.S., Zhu, R.X., Peng, S.Z., Wei, J.J., Yuan, B.Y., and Liu, T.S. 2002. Onset of Asian desertification by 22 Myr ago inferred from loess deposits in China. Nature, **416**: 159-163. doi:10.1038/416159a.

Hall, R. 1996. Reconstructing Cenozoic SE Asia. Geological Society, London, Special Publications, **106**: 153-184. doi:10.1144/GSL.SP.1996.106.01.11.

Hall, R. 2002. Cenozoic geological and plate tectonic evolution of SE Asia and the SW Pacific: computer-based reconstructions, model and animations. Journal of Asian Earth Sciences, **20**: 353-431. doi:10.1016/S1367-9120(01)00069-4.

Hall, R. 2012. Late Jurassic–Cenozoic reconstructions of the Indonesian region and the Indian Ocean. Tectonophysics, **570-571**: 1-41. doi:10.1016/j.tecto.2012.04.021.

Harris, S.E., and Mix, A.C. 1999. Pleistocene Precipitation Balance in the Amazon Basin Recorded in Deep Sea Sediments. Quat. res, **51**: 14-26. doi:10.1006/qres.1998.2008.

Harris, S.E., and Mix, A.C. 2002. Climate and tectonic influences on continental erosion of tropical South America, 0–13 Ma. Geology, **30**: 447–450. doi:10.1130/0091-7613(2002)030<0447:catioc>2.0.co;2.

Haug, G.H., and Tiedemann, R. 1998. Effect of the formation of the Isthmus of Panama on Atlantic Ocean thermohaline circulation. Nature, **393**: 673-676. doi:10.1038/31447.

Hilton, R.G., Galy, A., Hovius, N., Horng, M.-J., and Chen, H. 2010. The isotopic composition of particulate organic carbon in mountain rivers of Taiwan. Geochimica et Cosmochimica Acta, **74**: 3164-3181. doi:10.1016/j.gca.2010.03.004.

Horng, C.-S., and Shea, K.-S. 2007. The Quaternary magnetobiostratigraphy of Taiwan and Penglai orogenic events. Special Publication of the Central Geological Survey, **18**: 51-83.

Horng, C.-S., and Huh, C.-A. 2011. Magnetic properties as tracers for source-to-sink dispersal of sediments: A case study in the Taiwan Strait. Earth and Planetary Science Letters. doi:10.1016/j.epsl.2011.07.002.

Hsieh, A.I., Vaucher, R., Löwemark, L., Dashtgard, S.E., Horng, C.S., Lin, A.T.-S., and Zeeden, C. 2023a. Influence of a rapidly uplifting orogen on the preservation of climate oscillations. Paleoceanography and Paleoclimatology, **38**: e2022PA004586. doi:10.1029/2022PA004586.

Hsieh, A.I., Dashtgard, S.E., Wang, P.L., Horng, C.S., Su, C.C., Lin, A.T., Vaucher, R., and Löwemark, L. 2023b. Multi-proxy evidence for rapidly shifting sediment sources to the Taiwan Western Foreland Basin at the Miocene–Pliocene transition. Basin Research, **35**: 932-948. doi:10.1111/bre.12741.

Hsiung, K.-H., and Saito, Y. 2017. Sediment trapping in deltas of small mountainous rivers of southwestern Taiwan and its influence on East China Sea sedimentation. QUATERN INT, **455**: 30-44. doi:10.1016/j.quaint.2017.02.020.

Hu, D., Böning, P., Köhler, C.M., Hillier, S., Pressling, N., Wan, S., Brumsack, H.J., and Clift, P.D. 2012. Deep sea records of the continental weathering and erosion response to East Asian monsoon intensification since 14 ka in the South China Sea. Chemical Geology, **326-327**: 1-18. doi:10.1016/j.chemgeo.2012.07.024.

Hu, D., Clift, P.D., Böning, P., Hannigan, R., Hillier, S., Blusztajn, J., Wan, S., and Fuller, D.Q. 2013. Holocene evolution in weathering and erosion patterns in the Pearl River delta. Geochem. Geophys. Geosyst, **14**: 2349-2368. doi:10.1002/ggge.20166.

Hu, J., Kawamura, H., Li, C., Hong, H., and Jiang, Y. 2010. Review on current and seawater volume transport through the Taiwan Strait. J OCEANOGR, **66**: 591-610. doi:10.1007/s10872-010-0049-1.

Hu, S., Zeng, Z., Fang, X., Yin, X., Chen, Z., Li, X., Zhu, B., and Qi, H. 2020. Increasing terrigenous sediment supply from Taiwan to the southern Okinawa Trough over the last 3000 years evidenced by Sr Nd isotopes and geochemistry. Sedimentary Geology, **406**. doi:10.1016/j.sedgeo.2020.105725.

Jan, S., Wang, J., Chern, C.-S., and Chao, S.-Y. 2002. Seasonal variation of the circulation in the Taiwan Strait. J MARINE SYST, **35**: 249-268. doi:10.1016/S0924-7963(02)00130-6.

Jia, G., Peng, P.a., Zhao, Q., and Jian, Z. 2003. Changes in terrestrial ecosystem since 30 Ma in East Asia: Stable isotope evidence from black carbon in the South China Sea. Geology, **31**: 1093-1096. doi:10.1130/G19992.1.

Jian, Z., Yu, Y., Li, B., Wang, J., Zhang, X., and Zhou, Z. 2006. Phased evolution of the south–north hydrographic gradient in the South China Sea since the middle Miocene. Palaeogeography, Palaeoclimatology, Palaeoecology, **230**: 251-263. doi:10.1016/j.palaeo.2005.07.018.

Kämpf, N., and Schwertmann, U. 1983. Goethite and hematite in a climosequence in southern Brazil and their application in classification of kaolinitic soils. Geoderma, **29**: 27-39. doi:10.1016/0016-7061(83)90028-9.

Kao, S.-J., Jan, S., Hsu, S.-C., Lee, T.-Y., and Dai, M. 2008. Sediment Budget in the Taiwan Strait with High Fluvial Sediment Inputs from Mountainous Rivers: New Observations and Synthesis. Terrestrial, Atmospheric and Oceanic Sciences, **19**. doi:10.3319/TAO.2008.19.5.525(Oc).

Kao, S.J., and Liu, K.K. 2000. Stable carbon and nitrogen isotope systematics in a human-disturbed watershed (Lanyang-Hsi) in Taiwan and the estimation of biogenic particulate organic carbon and nitrogen fluxes. Global Biogeochemical Cycles, **14**: 189-198. doi:10.1029/1999gb900079.

Kao, S.J., and Milliman, J.D. 2008. Water and Sediment Discharge from Small Mountainous Rivers, Taiwan: The Roles of Lithology, Episodic Events, and Human Activities. The Journal of Geology, **116**: 431-448. doi:10.1086/590921.

Kao, S.J., Hilton, R.G., Selvaraj, K., Dai, M., Zehetner, F., Huang, J.C., Hsu, S.C., Sparkes, R., Liu, J.T., Lee, T.Y., Yang, J.Y.T., Galy, A., Xu, X., and Hovius, N. 2014. Preservation of terrestrial organic carbon in marine sediments offshore Taiwan: mountain building and atmospheric carbon dioxide sequestration. Earth Surface Dynamics, **2**: 127-139. doi:10.5194/esurf-2-127-2014.

Karl, D.M. 1999. A Sea of Change: Biogeochemical Variability in the North Pacific Subtropical Gyre. ECOSYSTEMS, **2**: 181-214. doi:10.1007/s100219900068.

Kissel, C., Liu, Z., Li, J., and Wandres, C. 2016. Magnetic minerals in three Asian rivers draining into the South China Sea: Pearl, Red, and Mekong Rivers. Geochemistry, Geophysics, Geosystems, **17**: 1678-1693. doi:10.1002/2016GC006283.

Kissel, C., Liu, Z., Li, J., and Wandres, C. 2017. Magnetic signature of river sediments drained into the southern and eastern part of the South China Sea (Malay Peninsula, Sumatra, Borneo, Luzon and Taiwan). Sedimentary Geology, **347**: 10-20. doi:10.1016/j.sedgeo.2016.11.007.
Kossin, J.P., Knapp, K.R., Olander, T.L., and Velden, C.S. 2020. Global increase in major tropical cyclone exceedance probability over the past four decades. Proceedings of the National Academy of Sciences, **117**: 11975-11980. doi:10.1073/pnas.1920849117.
Lan, J., Zhang, N., and Wang, Y. 2013. On the dynamics of the South China Sea deep circulation. J. Geophys. Res. Oceans, **118**: 1206-1210. doi:10.1002/jgrc.20104.
Lee, T.-Y., and Lawver, L.A. 1994. Cenozoic plate reconstruction of the South China Sea region. Tectonophysics, **235**: 149-180. doi:10.1016/0040-1951(94)90022-1.
Lee, T.-Y., Huang, J.-C., Lee, J.-Y., Jien, S.-H., Zehetner, F., and Kao, S.-J. 2015. Magnified Sediment Export of Small Mountainous Rivers in Taiwan: Chain Reactions from Increased Rainfall Intensity under Global Warming. PLoS One, **10**: e0138283. doi:10.1371/journal.pone.0138283.
Lepre, C.J., and Olsen, P.E. 2021. Hematite reconstruction of late triassic hydroclimate over the Colorado Plateau. Proceedings of the National Academy of Sciences, **118**. doi:10.1073/pnas.2004343118.
Li, B., Wang, J., Huang, B., Li, Q., Jian, Z., Zhao, Q., Su, X., and Wang, P. 2004. South China Sea surface water evolution over the last 12 Myr: A south-north comparison from Ocean Drilling Program Sites 1143 and 1146. Paleoceanography, **19**: PA1009. doi:10.1029/2003PA000906.
Liang, W.D., Tang, T.Y., Yang, Y.J., Ko, M.T., and Chuang, W.S. 2003. Upper-ocean currents around Taiwan. DEEP-SEA RES PT II, **50**: 1085-1105. doi:10.1016/S0967-0645(03)00011-0.
Lin, A.T.-S., and Watts, A.B. 2002. Origin of the West Taiwan basin by orogenic loading and flexure of a rifted continental margin. Journal of Geophysical Research: Solid Earth, **107**: ETG 2-1-ETG 2-19. doi:10.1029/2001jb000669.
Lin, A.T.-S., Watts, A.B., and Hesselbo, S.P. 2003. Cenozoic stratigraphy and subsidence history of the South China Sea margin in the Taiwan region. Basin Research, **15**: 453-478. doi:10.1046/j.1365-2117.2003.00215.x.
Lin, A.T.-S., Wang, S.-M., Hung, J.-H., Wu, M.-S., and Liu, C.-S. 2007. Lithostratigraphy of the Taiwan Chelungpu-Fault Drilling Project-A Borehole and Its Neighboring Region, Central Taiwan. Terrestrial, Atmospheric and Oceanic Sciences, **18**. doi:10.3319/tao.2007.18.2.223(tcdp).
Liu, C., Clift, P.D., Giosan, L., Miao, Y., Warny, S., and Wan, S. 2019. Paleoclimatic evolution of the SW and NE South China Sea and its relationship with spectral reflectance data over various age scales. Palaeogeography, Palaeoclimatology, Palaeoecology, **525**: 25-43. doi:10.1016/j.palaeo.2019.02.019.
Liu, C., Clift, P.D., Murray, R.W., Blusztajn, J., Ireland, T., Wan, S., and Ding, W. 2017. Geochemical evidence for initiation of the modern Mekong delta in the southwestern South China Sea after 8 Ma. Chemical Geology, **451**: 38-54. doi:10.1016/j.chemgeo.2017.01.008.
Liu, J., Chen, Z., Chen, M., Yan, W., Xiang, R., and Tang, X. 2010a. Magnetic susceptibility variations and provenance of surface sediments in the South China Sea. Sedimentary Geology, **230**: 77-85. doi:10.1016/j.sedgeo.2010.07.001.
Liu, J.P., Liu, C.S., Xu, K.H., Milliman, J.D., Chiu, J.K., Kao, S.J., and Lin, S.W. 2008. Flux and fate of small mountainous rivers derived sediments into the Taiwan Strait. Marine Geology, **256**: 65-76. doi:10.1016/j.margeo.2008.09.007.
Liu, Z., Alain, T., Clemens, S.C., and Wang, P. 2003. Quaternary clay mineralogy in the northern South China Sea (ODP Site 1146). Science in China Series D: Earth Sciences, **46**: 1223-1235. doi:10.1360/02yd0107.
Liu, Z., Zhao, Y., Colin, C., Siringan, F.P., and Wu, Q. 2009. Chemical weathering in Luzon, Philippines from clay mineralogy and major-element geochemistry of river sediments. Applied Geochemistry, **24**: 2195-2205. doi:10.1016/j.apgeochem.2009.09.025.
Liu, Z., Gan, J., Hu, J., Wu, H., Cai, Z., and Deng, Y. 2021. Progress on circulation dynamics in the East China Sea and southern Yellow Sea: Origination, pathways, and destinations of shelf currents. PROG OCEANOGR, **193**: 102553. doi:10.1016/j.pocean.2021.102553.
Liu, Z., Colin, C., Huang, W., Le, K.P., Tong, S., Chen, Z., and Trentesaux, A. 2007. Climatic and tectonic controls on weathering in south China and Indochina Peninsula: Clay mineralogical and geochemical investigations from the Pearl, Red, and Mekong drainage basins. Geochemistry, Geophysics, Geosystems, **8**: n/a-n/a. doi:10.1029/2006gc001490.

Liu, Z., Colin, C., Li, X., Zhao, Y., Tuo, S., Chen, Z., Siringan, F.P., Liu, J.T., Huang, C.-Y., You, C.-F., and Huang, K.-F. 2010b. Clay mineral distribution in surface sediments of the northeastern South China Sea and surrounding fluvial drainage basins: Source and transport. Marine Geology, **277**: 48-60. doi:10.1016/j.margeo.2010.08.010.

Liu, Z., Zhao, Y., Colin, C., Stattegger, K., Wiesner, M.G., Huh, C.-A., Zhang, Y., Li, X., Sompongchaiyakul, P., You, C.-F., Huang, C.-Y., Liu, J.T., Siringan, F.P., Le, K.P., Sathiamurthy, E., Hantoro, W.S., Liu, J., Tuo, S., Zhao, S., Zhou, S., He, Z., Wang, Y., Bunsomboonsakul, S., and Li, Y. 2016. Source-to-sink transport processes of fluvial sediments in the South China Sea. Earth-Science Reviews, **153**: 238-273. doi:10.1016/j.earscirev.2015.08.005.

Lüdmann, T., Wong, H.K., and Berglar, K. 2005. Upward flow of North Pacific Deep Water in the northern South China Sea as deduced from the occurrence of drift sediments. Geophysical Research Letters, **32**: 1-4. doi:10.1029/2004GL021967.

Lunt, D.J., Valdes, P.J., Haywood, A., and Rutt, I.C. 2008. Closure of the Panama Seaway during the Pliocene: implications for climate and Northern Hemisphere glaciation. Climate Dynamics, **30**: 1-18. doi:10.1007/s00382-007-0265-6.

Maher, B.A. 1986. Characterisation of soils by mineral magnetic measurements. Physics of the Earth and Planetary Interiors, **42**: 76-92. doi:10.1016/S0031-9201(86)8010-3.

Miller, K.G., Browning, J.V., Schmelz, W.J., Kopp, R.E., Mountain, G.S., and Wright, J.D. 2020. Cenozoic sea-level and cryospheric evolution from deep-sea geochemical and continental margin records. Science Advances, **6**: eaaz1346. doi:10.1126/sciadv.aaz1346.

Milliman, J.D., and Meade, R.H. 1983. World-wide delivery of river sediment to the oceans. The Journal of Geology, **91**: 1-21. doi:10.1086/628741.

Milliman, J.D., and Syvitski, J.P.M. 1992. Geomorphic/Tectonic Control of Sediment Discharge to the Ocean: The Importance of Small Mountainous Rivers. The Journal of Geology, **100**: 525-544. doi:10.1086/629606.

Milliman, J.D., and Farnsworth, K.L. 2011. River Discharge to the Coastal Ocean: A Global Synthesis. Cambridge University Press.

Milliman, J.D., Lin, S.W., Kao, S.J., Liu, J.P., Liu, C.S., Chiu, J.K., and Lin, Y.C. 2007. Short-term changes in seafloor character due to flood-derived hyperpycnal discharge: Typhoon Mindulle, Taiwan, July 2004. Geology, **35**. doi:10.1130/g23760a.1.

Nagel, S., Granjeon, D., Willett, S., Lin, A.T.-S., and Castelltort, S. 2018. Stratigraphic modeling of the Western Taiwan foreland basin: Sediment flux from a growing mountain range and tectonic implications. Marine and Petroleum Geology, **96**: 331-347. doi:10.1016/j.marpetgeo.2018.05.034.

Nagel, S., Castelltort, S., Wetzel, A., Willett, S.D., Mouthereau, F., and Lin, A.T. 2013. Sedimentology and foreland basin paleogeography during Taiwan arc continent collision. Journal of Asian Earth Sciences, **62**: 180-204. doi:10.1016/j.jseaes.2012.09.001.

Nan, F., Xue, H., and Yu, F. 2015. Kuroshio intrusion into the South China Sea: A review. PROG OCEANOGR, **137**: 314-333. doi:10.1016/j.pocean.2014.05.012.

Pan, T.-Y., Lin, A.T.-S., and Chi, W.-R. 2015. Paleoenvironments of the evolving Pliocene to early Pleistocene foreland basin in northwestern Taiwan: An example from the Dahan River section. Island Arc, **24**: 317-341. doi:10.1111/iar.12113.

Peterson, B.J., and Fry, B. 1987. Stable isotopes in ecosystem studies. Annual Review of Ecology and Systematics, **18**: 293-320. doi:10.1146/annurev.es.18.110187.001453.

Prell, W.L., and Kutzbach, J.E. 1992. Sensitivity of the Indian monsoon to forcing parameters and implications for its evolution. Nature, **360**: 647-352. doi:10.1038/360647a0.

Qu, T. 2000. Upper-layer circulation in the South China Sea. Journal of Physical Oceanography, **30**: 1450-1460. doi:10.1175/1520-0485(2000)030<1450:ULCITS>2.0.CO;2.

Qu, T., Mitsudera, H., and Yamagata, T. 1999. A Climatology of the Circulation and Water Mass Distribution near the Philippine Coast. Journal of Physical Oceanography, **29**: 1488-1505. doi:10.1175/1520-0485(1999)029<1488:ACOTCA>2.0.CO;2.

Qu, T., Girton, J.B., and Whitehead, J.A. 2006. Deepwater overflow through Luzon Strait. Journal of Geophysical Research, **111**: C01002. doi:10.1029/2005JC003139.

Qu, T., Kim, Y.Y., Yaremchuk, M., Tozuka, T., Ishida, A., and Yamagata, T. 2004. Can Luzon Strait Transport Play a Role in Conveying the Impact of ENSO to the South China Sea? Journal of Climate, **17**: 3644-3657. doi:10.1175/1520-0442(2004)017<3644:CLSTPA>2.0.CO;2.

Raymo, M.E. 1994. The Initiation of Northern Hemisphere Glaciation. Annual Review of Earth and Planetary Sciences, **22**: 353-383. doi:10.1146/annurev.ea.22.050194.002033.

Sarr, A.-C., Donnadieu, Y., Bolton, C.T., Ladant, J.-B., Licht, A., Fluteau, F., Laugié, M., Tardif, D., and Dupont-Nivet, G. 2022. Neogene South Asian monsoon rainfall and wind histories diverged due to topographic effects. Nature Geoscience, **15**: 314-319. doi:10.1038/s41561-022-00919-0.

Schlumberger. 1989. Log Interpretation Principles/Applications. Schlumberger, Houston.

Schroeder, A., Wiesner, M.G., and Liu, Z. 2015. Fluxes of clay minerals in the South China Sea. Earth and Planetary Science Letters, **430**: 30-42. doi:10.1016/j.epsl.2015.08.001.

Schwertmann, U. 1971. Transformation of Hematite to Goethite in Soils. Nature, **232**: 624-625. doi:10.1038/232624a0.

Shackleton, N.J., Backman, J., Zimmerman, H., Kent, D.V., Hall, M.A., Roberts, D.G., Schnitker, D., Baldauf, J.G., Desprairies, A., Homrighausen, R., Huddlestun, P., Keene, J.B., Kaltenback, A.J., Krumsiek, K.A.O., Morton, A.C., Murray, J.W., and Westberg-Smith, J. 1984. Oxygen isotope calibration of the onset of ice-rafting and history of glaciation in the North Atlantic region. Nature (London), **307**: 620-623. doi:10.1038/307620a0.

Shao, L., Qiao, P.-J., Pang, X., Wei, G.-J., Li, Q.-Y., Miao, W.-L., and Li, A. 2009. Nd isotopic variations and its implications in the recent sediments from the northern South China Sea. Chinese Science Bulletin, **54**: 311-317. doi:10.1007/s11434-008-0453-8.

Shaw, C.-L. 1996. Stratigraphic correlation and isopach maps of the Western Taiwan Basin. Terrestrial, Atmospheric, and Oceanic Sciences, **7**: 333-360. doi:doi:10.3319/TAO.1996.7.3.333(T).

Shipboard Scientific Party. 2000. Site 1148. *In* Wang, P., Prell, W.L., Blum, P., et al. Proceedings of the Ocean Drilling Program, Initial Reports, 184. pp. 1-121.

Sibuet, J.-C., and Hsu, S.-K. 2004. How was Taiwan created? Tectonophysics, **379**: 159-181. doi:10.1016/j.tecto.2003.10.022.

Steph, S., Tiedemann, R., Prange, M., Groeneveld, J., Schulz, M., Timmermann, A., Nürnberg, D., Rühlemann, C., Saukel, C., and Haug, G.H. 2010. Early Pliocene increase in thermohaline overturning: A precondition for the development of the modern equatorial Pacific cold tongue. Paleoceanography, **25**: n/a. doi:10.1029/2008PA001645.

Sun, D., Liu, D., Chen, M., An, Z., and Shaw, J. 1997. Magnetostratigraphy and palaeoclimate of Red Clay sequences from Chinese Loess Plateau. Science in China Series D: Earth Sciences, **40**: 337-343. doi:10.1007/BF02877564.

Sun, D., Shaw, J., An, Z., Cheng, M., and Yue, L. 1998. Magnetostratigraphy and paleoclimatic interpretation of a continuous 7.2 Ma Late Cenozoic Eolian sediments from the Chinese Loess Plateau. Geophysical Research Letters, **25**: 85-88. doi:10.1029/97GL03353.

Sun, X., and Wang, P.X. 2005. How old is the Asian monsoon system?—Palaeobotanical records from China. Palaeogeography, Palaeoclimatology, Palaeoecology, **222**: 181-222. doi:10.1016/j.palaeo.2005.03.005.

Sun, Y., An, Z., Clemens, S.C., Bloemendal, J., and Vandenberghe, J. 2010. Seven million years of wind and precipitation variability on the Chinese Loess Plateau. Earth and Planetary Science Letters, **297**: 525-535. doi:10.1016/j.epsl.2010.07.004.

Suppe, J. 1981. Mechanics of mountain building and metamorphism in Taiwan. Memoir of the Geological Society of China, **4**: 67-89.

Tamburini, F., Adatte, T., Föllmi, K., Bernasconi, S.M., and Steinmann, P. 2003. Investigating the history of East Asian monsoon and climate during the last glacial–interglacial period (0–140 000 years): mineralogy and geochemistry of ODP sites 1143 and 1144, South China Sea. Marine Geology, **201**: 147-168. doi:10.1016/S0025-3227(03)00214-7.

Teng, L.S. 1990. Geotectonic evolution of late Cenozoic arc-continent collision in Taiwan. Tectonophysics, **183**: 57-76. doi:doi:10.1016/0040-1951(90)90188-E.

Tensi, J., Mouthereau, F., and Lacombe, O. 2006. Lithospheric bulge in the West Taiwan Basin. Basin Research, **18**: 277-299. doi:10.1111/j.1365-2117.2006.00296.x.

Tian, J., Wang, P., Cheng, X., and Li, Q. 2005. Establishment of the Plio-Pleistocene as-tronomical timescale of ODP site 1143, Southern South China Sea. Journal of China University of Geosciences, **30**: 31-39.

Tian, J., Pak, D.K., Wang, P., Lea, D., Cheng, X., and Zhao, Q. 2006a. Late Pliocene monsoon linkage in the tropical South China Sea. Earth and Planetary Science Letters, **252**: 72-81. doi:10.1016 /j.epsl.2006.09.028.

Tian, J., Yang, Q., Liang, X., Xie, L., Hu, D., Wang, F., and Qu, T. 2006b. Observation of Luzon Strait transport. Geophys. Res. Lett, **33**: L19607-n/a. doi:10.1029/2006GL026272.

Tian, Z., Zhou, C., Xiao, X., Wang, T., Qu, T., Yang, Q., Zhao, W., and Tian, J. 2021. Water-Mass Properties and Circulation in the Deep and Abyssal Philippine Sea. Journal of geophysical research. Oceans, **126**: n/a. doi:10.1029/2020JC016994.

Vaucher, R., Dillinger, A., Hsieh, A.I., Chi, W.-R., Löwemark, L., and Dashtgard, S.E. 2023a. Storm-flood-dominated delta succession in the Pleistocene Taiwan Strait. The Depositional Record, **00**: 1-24. doi:10.1002/dep2.231.

Vaucher, R., Zeeden, C., Hsieh, A.I., Kaboth-Bahr, S., Lin, A.T., Horng, C.-S., and Dashtgard, S.E. 2023b. Hydroclimate dynamics during the Plio-Pleistocene transition in the northwest Pacific realm. Global and planetary change, **223**: 104088. doi:10.1016/j.gloplacha.2023.104088.

Vaucher, R., Dashtgard, S.E., Horng, C.S., Zeeden, C., Dillinger, A., Pan, Y.Y., Setiaji, R.A., Chi, W.R., and Lowemark, L. 2021. Insolation-paced sea level and sediment flux during the early Pleistocene in Southeast Asia. Scientific Reports, **11**: 16707. doi:10.1038/s41598-021-96372-x.

Wan, S., Li, A., Clift, P.D., and Jiang, H. 2006. Development of the East Asian summer monsoon: Evidence from the sediment record in the South China Sea since 8.5 Ma. Palaeogeography, Palaeoclimatology, Palaeoecology, **241**: 139-159. doi:10.1016/j.palaeo.2006.06.013.

Wan, S., Li, A., Clift, P.D., and Stuut, J.-B.W. 2007. Development of the East Asian monsoon: Mineralogical and sedimentologic records in the northern South China Sea since 20 Ma. Palaeogeography, Palaeoclimatology, Palaeoecology, **254**: 561-582. doi:10.1016 /j.palaeo.2007.07.009.

Wan, S., Tian, J., Steinke, S., Li, A., and Li, T. 2010a. Evolution and variability of the East Asian summer monsoon during the Pliocene: Evidence from clay mineral records of the South China Sea. Palaeogeography, Palaeoclimatology, Palaeoecology, **293**: 237-247. doi:10.1016/j.palaeo.2010.05.025.

Wan, S., Li, A., Clift, P.D., Wu, S., Xu, K., and Li, T. 2010b. Increased contribution of terrigenous supply from Taiwan to the northern South China Sea since 3Ma. Marine Geology, **278**: 115-121. doi:10.1016/j.margeo.2010.09.008.

Wang, G., Xie, S.-P., Qu, T., and Huang, R.X. 2011. Deep South China Sea circulation. Geophysical Research Letters, **38**: L05601. doi:10.1029/2010GL046626.

Wang, H., Lu, H., Zhao, L., Zhang, H., Lei, F., and Wang, Y. 2019. Asian monsoon rainfall variation during the Pliocene forced by global temperature change. Nature Communications, **10**: 5272. doi:10.1038/s41467-019-13338-4.

Wang, P., and Li, Q. 2009. Oceanographical and Geological Background. *In* The South China Sea. *Edited by* P. Wang and Q. Li. Springer, Dordrecht. pp. 25-73.

Wang, P., Prell, W.L., and Blum, P. 2005a. Magnetic susceptibility on ODP Hole 184-1143C. *In* Shipboard Scientific Party, PANGAEA.

Wang, P., Clemens, S., Beaufort, L., Braconnot, P., Ganssen, G., Jian, Z., Kershaw, P., and Sarnthein, M. 2005b. Evolution and variability of the Asian monsoon system: state of the art and outstanding issues. Quaternary Science Reviews, **24**: 595-629. doi:10.1016/j.quascirev.2004.10.002.

Webster, P.J. 1994. The role of hydrological processes in ocean-atmosphere interactions. Reviews of Geophysics, **32**: 427-476. doi:10.1029/94RG01873.

Wilkens, R.H., Westerhold, T., Drury, A.J., Lyle, M., Gorgas, T., and Tian, J. 2017. Revisiting the Ceara Rise, equatorial Atlantic Ocean: isotope stratigraphy of ODP Leg 154 from 0 to 5 Ma. Climate of the Past, **13**: 779-793. doi:10.5194/cp-13-779-2017.

Xin, S., Shen, J., Zhang, W., Sun, W., and Xiao, X. 2020. East Asian winter monsoon evolution since the late Pliocene based on a pollen record from Lake Xingkai, northeast Asia. Quaternary Research, **93**: 40-59. doi:10.1017/qua.2019.45.

Yan, Q., Wei, T., Zhang, Z., and Jiang, N. 2019a. Orbitally Induced Variation of Tropical Cyclone Genesis Potential Over the Western North Pacific During the Mid-Piacenzian Warm Period: A Modeling Perspective. Paleoceanography and Paleoclimatology, **34**: 902-916. doi:10.1029/2018pa003535.

Yan, Q., Korty, R., Zhang, Z., and Wang, H. 2019b. Evolution of tropical cyclone genesis regions during the Cenozoic era. Nature Communications, **10**. doi:10.1038/s41467-019-11110-2.

Yan, Q., Wei, T., Korty, R.L., Kossin, J.P., Zhang, Z., and Wang, H. 2016. Enhanced intensity of global tropical cyclones during the mid-Pliocene warm period. Proceedings of the National Academy of Sciences, **113**: 12963-12967. doi:10.1073/pnas.1608950113.

Yin, S., Hernández-Molina, F.J., Lin, L., Chen, J., Ding, W., and Li, J. 2021. Isolation of the South China Sea from the North Pacific Subtropical Gyre since the latest Miocene due to formation of the Luzon Strait. Scientific Reports, **11**: 1562-1562. doi:10.1038/s41598-020-79941-4.

Yin, S., Hernández-Molina, F.J., Lin, L., He, M., Gao, J., and Li, J. 2023. Plate convergence controls long-term full-depth circulation of the South China Sea. Marine Geology, **459**: 107050. doi:10.1016/j.margeo.2023.107050.

Yu, H.-S., and Chou, Y.-W. 2001. Characteristics and development of the flexural forebulge and basal unconformity of Western Taiwan Foreland Basin. Tectonophysics, **333**: 277-291. doi:doi:10.1016/S0040-1951(00)00279-1.

Zhang, W., Wei, X., Jinhai, Z., Yuliang, Z., and Zhang, Y. 2012. Estimating suspended sediment loads in the Pearl River Delta region using sediment rating curves. Continental Shelf Research, **38**: 35-46. doi:10.1016/j.csr.2012.02.017.

Zhang, Y., Zhang, Z., Chen, D., Qiu, B., and Wang, W. 2020. Strengthening of the Kuroshio current by intensifying tropical cyclones. Science, **368**: 988-993. doi:10.1126/science.aax5758.

Zhang, Y., Liu, Z., Zhao, Y., Wang, W., Li, J., and Xu, J. 2014. Mesoscale eddies transport deep-sea sediments. Scientific Reports, **4**: 5937-5937. doi:10.1038/srep05937.

Zhang, Y.G., Ji, J., Balsam, W.L., Liu, L., and Chen, J. 2007. High resolution hematite and goethite records from ODP 1143, South China Sea: Co-evolution of monsoonal precipitation and El Niño over the past 600,000 years. Earth and Planetary Science Letters, **264**: 136-150. doi:10.1016/j.epsl.2007.09.022.

Zhang, Y.G., Ji, J., Balsam, W., Liu, L., and Chen, J. 2009. Mid-Pliocene Asian monsoon intensification and the onset of Northern Hemisphere glaciation. Geology, **37**: 599-602. doi:10.1130/g25670a.1.

Zhao, W., Zhou, C., Tian, J., Yang, Q., Wang, B., Xie, L., and Qu, T. 2014. Deep water circulation in the Luzon Strait. Journal of Geophysical Research, **119**: 790-804. doi:10.1002/2013JC009587.

Zhong, Y., Wilson, D.J., Liu, J., Wan, S., Bao, R., Liu, J., Zhang, Y., Wang, X., Liu, Y., Liu, X., Zhao, Y., Li, S., and Liu, Q. 2021. Contrasting Sensitivity of Weathering Proxies to Quaternary Climate and Sea-Level Fluctuations on the Southern Slope of the South China Sea. Geophysical Research Letters, **48**: n/a. doi:10.1029/2021GL096433.

Zhou, C., Zhao, W., Tian, J., Zhao, X., Zhu, Y., Yang, Q., and Qu, T. 2017. Deep Western Boundary Current in the South China Sea. Scientific Reports, **7**: 9303-9307. doi:10.1038/s41598-017-09436-2.

Zhou, X., Yang, J., Xiao, G., Wang, J., Hu, Y., Zheng, Y., Liu, J., and Li, X. 2023. Megacycles of climate and vegetation in East Asia since 3 Ma. Catena (Giessen), **229**: 107195. doi:10.1016/j.catena.2023.107195.

Zhu, Y., Sun, J., Wang, Y., Li, S., Xu, T., Wei, Z., and Qu, T. 2019. Overview of the multi-layer circulation in the South China Sea. Progress in Oceanography, **175**: 171-182. doi:10.1016/j.pocean.2019.04.001.